Bending and free vibration analysis of functionally graded sandwich plates: An assessment of the Refined Zigzag Theory

Bending and free vibration analysis of functionally graded sandwich plates: An assessment of the Refined Zigzag Theory

M. Di Sciuva and M. Sorrenti[1]

Department of Mechanical and Aerospace Engineering – Politecnico di Torino

Corso Duca degli Abruzzi, 24 10129 Torino, Italy

e-mails: marco.disciuva@polito.it, matteo.sorrenti@polito.it

Abstract.

The paper presents a numerical assessment of the performance of the Refined Zigzag Theory (RZT) to the analysis of bending (deflection and stress distributions) and free vibration of functionally graded materials (FGM) plates, monolayer and sandwich, under a set of different boundary conditions. The numerical assessment is performed comparing results from RZT using Ritz method with those from 3-D, quasi 3-D and 2-D theories and finite element method (FEM). In the framework of 2D theories, equivalent single layer theories (ESL) of different order (sinusoidal, hyperbolic, inverse- hyperbolic, third-order (TSDT), first-order (FSDT) and classical (CPT)) have been used to investigate deformation, stresses, and free vibration and compared with results from the RZT.

After validating the convergence characteristics and the numerical accuracy of the developed approach using orthogonal admissible functions, a detailed parametric numerical investigation is carried out. Bending under transverse pressure and free vibration of FGM square and rectangular plates of different aspect ratio under various combinations of geometry (core-to-face sheet thickness ratio and plate to thickness ratio), boundary conditions and law of variation of volume fraction constituent in the thickness direction (power-law (P-FGM), exponential law (E-FGM) and sigmoidal-law (S-FGM)) is studied. Monolayer and sandwich plates with homogeneous core and functionally graded face-sheets are considered for the assessment. It is concluded that the RZT generally predicts the global (deflection and frequencies) and local (displacement and stress distributions) response of FGM sandwich plates, more accurately than first-order (FSDT) and third-order (TSDT) shear deformation theories, while retaining its simplicity.

***Keywords*:** Composite multilayer and sandwich plates; functionally graded materials; Refined Zigzag Theory; bending; vibration; Ritz method.

[1] Corresponding Author: Matteo Sorrenti, email: matteo.sorrenti@polito.it Tel. +39 3337120343.

1. **Introduction**

Thanks to their superior characteristics of specific stiffness and strength, as well as high damping and good fatigue properties compared to traditional metallic materials, glass or carbon fibers reinforced polymer matrix (FRP) composites have registered in the last decades sustained and increased application to military and civilian aircraft, aerospace vehicles, automotive, naval, and civil structures. Alongside their interesting features, the FRP-composites suffer from some weaknesses. As it is well known, FRP-composite structures are produced by bonded unidirectional or woven layers with angles of orientation of the fibers generally varying from layer to layer. Thus, a through-the-thickness piecewise constant distribution of mechanical and thermal properties takes place. The abrupt change in mechanical and thermal properties from one layer to the adjacent one generally causes a stress concentration at the layer interface that can initiate delamination. Another weakness concerns the imperfect bonding of the layers and the imperfect adherence between fibers and matrix. All this leads to a more or less severe degradation of the actual mechanical characteristics compared to the nominal ones of the FRP-composites [1]. For the same reasons, classical sandwich constructions which usually consist of a thick low strength core and two thin stiff outer face sheets, suffer the same weaknesses.

Developed during 1980s at the Japanese Aerospace Laboratory under the impulse of Japanese national space research program of reusable rocket engines for space plane [2, 3], the functionally graded materials (FGMs) are advanced composite materials made by two or more phases mixed together in order to obtain a synergic combination of their mechanical and thermal properties. Without loss of generality, FGMs are particular composites in which the fraction volume of the two or more phases varies along the grading direction according to an appropriate law, aimed to tailor in that direction the distribution of those features (such as Young's modulus, shear modulus, Poisson's ratio, thermal expansion coefficients, material density) significant for the specific application (spacecraft heat shields, flywheels, nuclear components for fusion reactors, high temperature thermal barrier coatings, heat exchanger tubes, biomedical implants, etc), [4–7].

Contrary to the FRP-composites, the FGMs feature a continuous and smooth variation of the properties along the grading direction, typically the thickness in plate/shell like structures. Thanks to the smooth continuous distribution of properties along the thickness of each layer, the FGMs can either reduce or remove the discontinuity at layer interfaces and core-face sheets interfaces in classical sandwich constructions, thus enhancing the delamination resistance. Other advantages of FGMs over to the traditional FRP-composites pertain the reduction of the in-plane stresses, an enhancement of residual stresses and thermal properties, an increase of fracture toughness and a reduction of the stress intensity factors, Birman [8].

FGMs, like FRP-composites, are considered macroscopically heterogeneous materials whose effective mechanical and thermal characteristics are derived by means of appropriate homogenization techniques. The choice of an homogenization scheme should be made carefully since it may affect the response predictions, [9–16].

As an alternative to the micromechanics-based homogenization techniques, Mori-Tanaka approach or Halpin-Tsai model [17–26], the rule of mixtures (Voigt model) is the most popular and commonly used model to estimate the distribution of the effective mechanical and thermal characteristics along the grading direction, [16, 27–37]. Three laws of distribution are commonly used: a power-law (P-FGM), an exponential law (E-FGM) and a sigmoidal-law (S-FGM), [36–43]. The shape of these laws is tuned by a coefficient, referred in the literature as either grading index or power law index. Acting on this index, one could tailor the FGM properties and optimize the material for its specific application.

Sandwich constructions appear to be the natural candidates to the introduction of advanced composite materials [44]. Sandwich beams, plates and shells with FGMs face-sheets or cores have been extensively studied in the last two decades [8, 45, 46], both using 3D, quasi-3D and 2D approaches, coupled with various analytical and numerical methods. 3D elasticity solutions have been obtained in Refs. [47–52]. Quasi-3D higher-order, sinusoidal and hyperbolic theories have been used in Refs. [53–58] to study FGMs plates. In the framework of 2D approaches, equivalent single layer theories (see, [59, 60]) of different order (sinusoidal, hyperbolic, *n*-order, third-order shear deformation (TSDT), first-order shear deformation (FSDT and classical (CPT) plate theories, [20–24, 28, 30, 31, 37, 43, 47, 61–81], layer-wise [26, 32, 34, 82] and zigzag theories [29, 81, 83–86] have been used to investigate deformation, stresses, free vibration, buckling and post-buckling, of FGMs sandwich plates. For a recent review on this topic the reader is encouraged to refer to Thai et al [45]. Concerning the solution methods, the Ritz method in conjunction with Chebyshev polynomials as coordinate functions multiplied by appropriate boundary functions in order to satisfy the geometric boundary conditions has been used to perform a three-dimensional analysis of the displacements and stresses of fully clamped functionally graded plates subjected to a uniform load on the top surface by Elishakoff et al [87], and to investigate the vibration of P-FGM sandwich plates, both simply supported and clamped by Li et al [50]. Iurlaro et al [86] employed the Refined zigzag theory with Navier solution and the Ritz method. Rayleigh-Ritz method and P-FGM has been used by Pradhan et al [66] in investigating the free-vibration of Euler and Timoshenko FGM beams. Kumar [88] performed the analysis of free vibration of two-directional FGMs annular plates using Chebyshev collocation technique and Differential Quadrature Method (DQM). Das et al [89] developed a triangular plate element for the thermo-mechanic analysis of sandwich plates with functionally graded core based on an higher-order model. Based on a *n*th-order shear deformation theory, Xiang et al. [69, 90, 91] investigated the behavior of free vibration of sandwich plates with functionally graded face-sheets and homogeneous core by using the meshless global radial basis function collocation method based on the thin plate spline radial basis function and *n*th-order shear deformation theory. Zhao et

al [92] used the FSDT and the element-free *kp*-Ritz method to study the free vibration of FGM plates with different boundary conditions. Zuo et al [93] used the wavelet finite element method to investigate free vibration and buckling of functionally graded plates. Based on the first-order shear deformation theory (FSDT), Reddy [47] and Srividhya et al [16] developed a four-node C^0 plate element. Gupta et al [94–96] developed a nine node with eight nodal degrees of freedom C^0 element. Natarajan et al [83] investigated the bending and the free flexural vibration behaviour of sandwich functionally graded material (FGM) plates using QUAD-8 shear flexible element developed based on higher order zig-zag theory. The thermal effect on the response of FGMs structures has been investigated by many researchers. For a critical review on this topic, the interested reader is encouraged to refer to Swaminathan et al [6]. The impact response and wave propagation have been studied in [79, 97, 98]. For a literature review on thermal stability analysis of plates with functionally graded coefficient of thermal expansion, see Bousahla et al [99].

Reviews concerning modeling and analysis of FGM sandwich beams can be found in Refs [46, 100]; for cylindrical structures with an emphasis on coupled mechanics, including thermo-elastic coupling, multi-physic fields coupling, structure–foundation coupling and fluid–solid coupling, see Dai et al [101].

From the previous literature survey, though by no means exhaustive, it appears that a large number of ESL theories were used in the analysis of the thermo-structural behavior of FGMs beams, plates and shells. There are few papers that have made use of layer-wise and zigzag plate theories. Regarding solution methods, in addition to the classical methods (Navier and finite element method), an increasing number of researchers used the Rayleigh-Ritz method, [102, 103].

In the framework of zigzag theories, Tessler et al. formulated the Refined Zigzag Theory (RZT), a zigzag model suitable for the analysis of traditional multilayered composite and sandwich beams, [104–106], plates [107, 108] and shells [109]. The kinematics is comprised of two contributions: the global kinematics given by the FSDT, enriched by adding a through the thickness piecewise linear (local kinematics) zigzag function in the in-plane displacements. The resulting kinematics has a fixed number of kinematic unknowns, regardless of the number of layers, and does not require any shear correction factor.

Numerical tests on bending, free vibrations and buckling of rectangular sandwich plates subjected to several combinations of loads and boundary conditions have shown the remarkable accuracy of the RZT, also for laminates and sandwich with weak external layers, [86, 110–112]. From a numerical point of view, RZT allows for the formulation of C^0 continuity finite elements, [112–122].

The previous bibliographic survey shows that to date there has not yet been a thorough numerical assessment of the performance of the Refined Zigzag Theory (RZT) to the analysis of bending (deflection and stress distributions) and free vibration of functionally graded materials (FGM) plates, laminated composite and sandwich, under a set of different boundary conditions. The purpose of the present work is to fill this gap.

It should be noted that the dependence of the elastic moduli on the thickness co-ordinate in FGM layers make the standard RZT not applicable in a straight-forward manner. Iurlaro et al [86] have been used the RZT for the analysis of composite and sandwich structures with FGM layers.

The present work is organized as follows.

In Sect. 2, the general theory and the governing equations are derived. First, the RZT is presented; based on the RZT kinematics, the discrete governing equations for bending and free vibration analysis of functionally graded multilayered composite and sandwich plates are derived directly from the principle of virtual work.

The effective material properties (Young's moduli and mass density) of the FGMs in the x_3-direction are derived using the extended rule of moistures. Three laws of variation of volume fraction in the thickness direction are used: power-law (P-FGM), exponential law (E-FGM) and sigmoidal-law (S-FGM).

Sect. 3 presents numerical studies.

First, convergence analysis results of the Ritz method in conjunctions with orthogonal admissible functions are presented and discussed.

Subsequently, in order to validate the predictive capability of the RZT for the problems at hand, comparative numerical studies are performed using 3D elasticity, whenever available, First-order Shear Deformation Theory-FSDT (using standard and ad-hoc transverse shear correction factors) and Third-order Shear Deformation Theory-TSDT, and non-polynomial theories.

It is concluded that the RZT generally predicts the global (deflection and frequencies) and local (displacement and stress distributions) response of FGM sandwich plates, more accurately than first-order (FSDT) and third-order (TSDT) shear deformation theories, while retaining its simplicity.

In Sect.4, some conclusions are presented based on the numerical investigations performed.

In Appendix, the assumed orthogonal trial functions used in the Ritz method are discussed, in conjunction with the Gram-Schmidt orthogonalization method.

2 Governing equations

2.1 Geometrical preliminaries

We consider a rectangular multilayered flat plate made of a finite number *N* of perfectly bonded layers. *V* is the volume of the plate, *h* the thickness, *a* the length and *b* the width. The thickness of each layer, as well as of the whole plate, is assumed to be constant, and the material of each layer is assumed to be linearly elastic and orthotropic with a plane of elastic symmetry parallel to the reference surface and whose principal orthotropy directions are arbitrarily oriented with respect to the reference frame. The points of the plate are referred to an orthogonal Cartesian co-ordinate system

$\mathbf{X} = x_j \quad (j = 1,2,3)$, where $\mathbf{x} = x_\alpha \quad (\alpha = 1,2)$ is the set of in-plane co-ordinates on the reference plane, here chosen to be the middle plane of the plate, and $x_3 \equiv z$ is the co-ordinate normal to the reference plane (Fig. 1); the origin of the reference frame is fixed at the center of the middle-plane of the plate, so that, x_1 is defined in the range $x_1 \in \left[-\frac{a}{2}, +\frac{a}{2}\right]$, x_2 in the range $x_2 \in \left[-\frac{b}{2}, +\frac{b}{2}\right]$, and x_3 in the range $x_3 \in \left[-\frac{h}{2}, +\frac{h}{2}\right]$. In the body of paper, also the following nondimensional co-ordinates will be adopted $(\xi_1, \xi_2) = \left(\frac{2x_1}{a}, \frac{2x_2}{b}\right) \in [-1, +1]$.

If not otherwise stated, in the paper the superscript (*k*) is used to indicate quantities corresponding to the *k*th layer (*k*=1,N), whereas the subscript (*k*) defines quantities corresponding to the *k*th interface (*k*=1,N-1) between the *k* and (*k+1*) layer. So, in the following, the symbol $(.)_{(k)}$ stands for (.) valued at $x_3 = z_{(k)}$, i.e., at the *k*-th interface. Also, we use the subscript *b* and *t* to indicate the top and bottom surfaces of the plate; specifically, $z_{(0)} = z_b$ and $z_{(N)} = z_t$ denote the co-ordinates of the bottom and top surfaces of the whole plate; thus, $h = z_t - z_b$ is the plate thickness and $h^{(k)} = z_{(k)} - z_{(k-1)} \ (k = 1,2,...,N)$, the thickness of the *k*th layer (see Figure 1).

The plate is subjected to a transverse load $\overline{p}_z$ applied on the top surface of the plate, and to uniformly distributed in-plane edge loads for unit length ($\overline{P}_{xx}$, $\overline{P}_{yy}$, $\overline{P}_{xy}$) and boundary transverse loads ($\overline{P}_{13}$, $\overline{P}_{23}$), applied along the edges $x_1 = \pm\frac{a}{2}$ and $x_2 = \pm\frac{b}{2}$, respectively (see, Figure 1).

The symbol $(\bullet)_{,i} = \frac{\partial(\bullet)}{\partial x_i}$ refer to the derivative of the function $(\bullet)$ with respect to the coordinate x_i, i.e., $(\bullet)_{,i} = \frac{\partial(\bullet)}{\partial x_i}$.

In the paper, if not otherwise specified, the Einstenian summation convention over repeated indices is adopted, with Latin indices ranging from 1 to 3, and Greek indices ranging from 1 to 2.

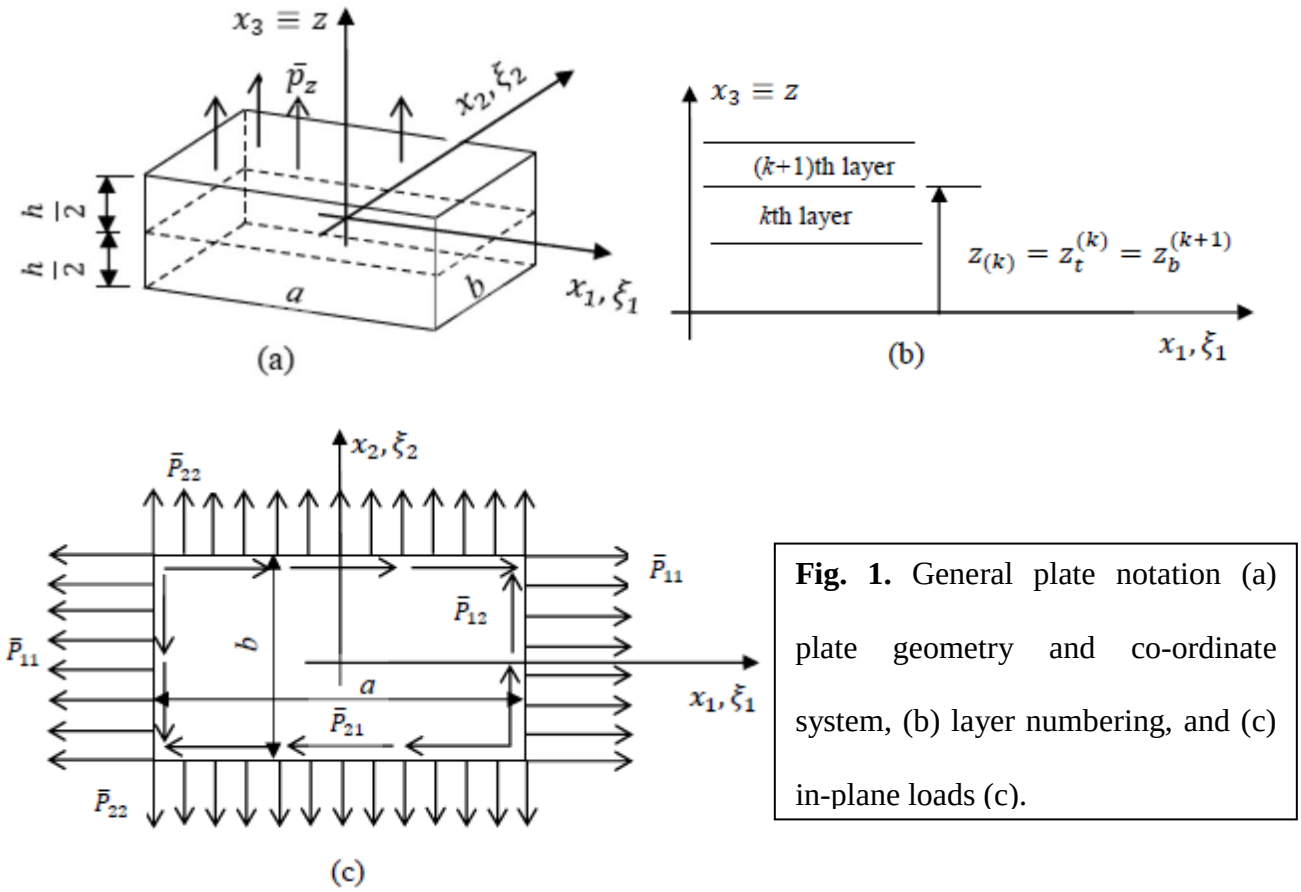

Fig. 1. General plate notation (a) plate geometry and co-ordinate system, (b) layer numbering, and (c) in-plane loads (c).

2.2 Homogenization of material properties

It is assumed that the functionally graded layers are made from a mixture of two phases. The effective material properties of the two-phase layer can be estimated according to the Mori–Tanaka scheme or the Voigt model (rule of mixtures (ROM)), Refs. [13, 14, 47, 61]. Due to its simplicity, in the present study the ROM is used to obtain the equivalent properties of the FGMs.

As we said, there are three different types of law of variation of the properties through the thickness of the layer in the literature, [36–43]: exponential (E-FGM), power series (P-FGM) and sigmoidal law (S-FGM). In this study, all of these laws are considered.

Table 1 gives the three law of variation of the property $P^{(k)}(z)$ within the layer *k*th as a function of the z-coordinate;

$h^{(k)} = z_t^{(k)} - z_b^{(k)}$ and $z_M^{(k)} = \dfrac{z_t^{(k)} + z_b^{(k)}}{2}$ are the thickness and the co-ordinate of the middle plane of the *k*th layer here assumed as reference plane). *p*, the volume fraction exponent, also referred to as the gradient (power-law) index in the literature, is a non-negative variable parameter, $p \geq 0$. It dictates the material variation profile through the thickness. Moreover,

$$V_t^{(k)} = \left(\frac{1}{2} + \frac{z - z_M^{(k)}}{h^{(k)}} \right)^p \tag{1}$$

is the volume fraction of the property on the top surface, $P_t^{(k)}$.

Note that $V_b^{(k)} + V_t^{(k)} = 1$, so

$$V_b^{(k)} = 1 - \left(\frac{1}{2} + \frac{z - z_M^{(k)}}{h^{(k)}} \right)^p \tag{2}$$

is the volume fraction of the property on the bottom surface, $P_b^{(k)}$.

Note also that

$$f_1^{(k)}(z) = f_2^{(k)}(z) = V_t^{(k)} \quad \text{for } p = 1. \tag{3}$$

So, S-FGM law is the same as P-FGM law for *p*=1.

Table 1. Variation laws as a function of the z-coordinate (layer *k*th of thickness $h^{(k)}$; reference plane is the middle plane).

P-FGM	$P^{(k)}(z) = \left(P_t^{(k)} - P_b^{(k)} \right) V_t^{(k)} + P_b^{(k)} \quad 0 \le p \le \infty$
E-FGM	$P^{(k)}(z) = P_b^{(k)} e^{\left(\ln \frac{P_t^{(k)}}{P_b^{(k)}} \right) V_t^{(k)}}$
S-FGM	$P^{(k)}(z) = f_1^{(k)}(z) P_t^{(k)} + \left(1 - f_1^{(k)}(z) \right) P_b^{(k)} \quad \text{for} \quad z_M^{(k)} \le z \le z_t^{(k)}$ $P^{(k)}(z) = f_2^{(k)}(z) P_t^{(k)} + \left(1 - f_2^{(k)}(z) \right) P_b^{(k)} \quad \text{for} \quad z_b^{(k)} \le z \le z_M^{(k)}$ $f_1^{(k)}(z) = 1 - \frac{1}{2} \left(1 - 2 \frac{\left(z - z_M^{(k)} \right)}{h^{(k)}} \right)^p \; ; \quad f_2^{(k)}(z) = \frac{1}{2} \left(1 + 2 \frac{\left(z - z_M^{(k)} \right)}{h^{(k)}} \right)^p$

2.3 Kinematics

In this paper, the kinematics of the Refined Zigzag Theory proposed by Tessler et al [104–108] and adopted by Iurlaro et al [86] to take into account layers made up of functionally graded materials, is adopted. The theory is based

on the superposition of a global (*G*) first–order kinematics (that of Mindlin's plate theory, FSDT) and a local (*L*) layer-wise correction of the in-plane displacements. Thus, the displacement field at time *t* is written as

$$\begin{Bmatrix} \tilde{u}_1(x_j,t) \\ \tilde{u}_2(x_j,t) \\ \tilde{u}_3(x_j,t) \end{Bmatrix} = \begin{Bmatrix} u_1^G(x_j,t) \\ u_2^G(x_j,t) \\ u_3^G(x_j,t) \end{Bmatrix} + \begin{Bmatrix} u_1^L(x_j,t) \\ u_2^L(x_j,t) \\ 0 \end{Bmatrix} \tag{4}$$

where

$$\begin{Bmatrix} u_1^G(x_j,t) \\ u_2^G(x_j,t) \\ u_3^G(x_j,t) \end{Bmatrix} = \begin{Bmatrix} u_1(x_\beta,t) \\ u_2(x_\beta,t) \\ w(x_\beta,t) \end{Bmatrix} + z \begin{Bmatrix} \theta_1(x_\beta,t) \\ \theta_2(x_\beta,t) \\ 0 \end{Bmatrix} \tag{5}$$

gives the contribution which is continuous with its first derivatives with respect to the z-coordinate and

$$\begin{Bmatrix} u_1^{L(k)}(x_j,t) \\ u_2^{L(k)}(x_j,t) \\ u_3^{L(k)}(x_j,t) \end{Bmatrix} = \begin{Bmatrix} \phi_1^{(k)}(z)\psi_1(x_\beta,t) \\ \phi_2^{(k)}(z)\psi_2(x_\beta,t) \\ 0 \end{Bmatrix} \tag{6}$$

gives the contribution to the in-plane displacement which is continuous with respect to x_3, but with jumps in the first derivative at the interfaces between adjacent layers.

In compact matrix format,

$$\begin{aligned} \tilde{\mathbf{u}}(x_j,t) &= \mathbf{u}^G(x_j,t) + \mathbf{u}^L(x_j,t) \\ \tilde{u}_3(x_j,t) &= u_3^G(x_j,t) \end{aligned} \tag{4a}$$

$$\begin{aligned} \mathbf{u}^G(x_j,t) &= \mathbf{u}(x_\beta,t) + z\boldsymbol{\theta}(x_\beta,t) \\ u_3^G(x_j,t) &= w(x_\beta,t) \end{aligned} \tag{5a}$$

$$\mathbf{u}^{L(k)}(x_j,t) = \boldsymbol{\phi}^{(k)}(z)\boldsymbol{\psi}(x_\beta,t) \tag{6a}$$

In the previous equations, u_1 and u_2 are the displacements along the x_1- and x_2- axis of a point belonging to the middle plane of the plate; θ_1 and θ_2 are the bending rotation of the normal to the middle surface along the directions $+x_2$ and $-x_1$, respectively, and *w* is the transverse deflection, assumed to be constant along the thickness. ψ_1 and ψ_2 represent the spatial amplitudes of the zigzag functions $\phi_1^{(k)}$ and $\phi_2^{(k)}$, respectively. It should be noted that FSDT is a special case of the RZT, i.e., RZT reduces to FSDT for $\boldsymbol{u}^{L(k)} = \mathbf{0}$ (see, Eqs. (4) and (5)).

2.4 Strain-displacement relations

The linear strain expressions associated with the displacement field in Eq. (4) are:

$$\begin{Bmatrix} \tilde{\varepsilon}_{11} \\ \tilde{\varepsilon}_{22} \\ \tilde{\gamma}_{12} \end{Bmatrix}^{(k)} = \begin{Bmatrix} \tilde{u}_{1,1} \\ \tilde{u}_{2,2} \\ \tilde{u}_{1,2}+\tilde{u}_{2,1} \end{Bmatrix} = \begin{Bmatrix} u_{1,1} \\ u_{2,2} \\ u_{1,2}+u_{2,1} \end{Bmatrix} + z \begin{Bmatrix} \theta_{1,1} \\ \theta_{2,2} \\ \theta_{1,2}+\theta_{2,1} \end{Bmatrix} + \begin{bmatrix} \phi_1^{(k)} & 0 & 0 & 0 \\ 0 & 0 & 0 & \phi_2^{(k)} \\ 0 & \phi_2^{(k)} & \phi_1^{(k)} & 0 \end{bmatrix} \begin{Bmatrix} \psi_{1,1} \\ \psi_{2,1} \\ \psi_{1,2} \\ \psi_{2,2} \end{Bmatrix} \tag{7}$$

$$\begin{Bmatrix} \tilde{\gamma}_{13} \\ \tilde{\gamma}_{23} \end{Bmatrix}^{(k)} = \begin{Bmatrix} u_{1,3}+w_{,1} \\ u_{2,3}+w_{,2} \end{Bmatrix}^{(k)} = \begin{Bmatrix} \theta_1+\phi_{1,3}^{(k)}\psi_1+w_{,1} \\ \theta_2+\phi_{2,3}^{(k)}\psi_2+w_{,2} \end{Bmatrix} = \begin{Bmatrix} \theta_1+w_{,1} \\ \theta_2+w_{,2} \end{Bmatrix} + \begin{bmatrix} \phi_{1,3}^{(k)} & 0 \\ 0 & \phi_{2,3}^{(k)} \end{bmatrix} \begin{Bmatrix} \psi_1 \\ \psi_2 \end{Bmatrix} \tag{8}$$

In compact matrix format,

$$\tilde{\boldsymbol{\varepsilon}} = \boldsymbol{\varepsilon}_m + z\boldsymbol{\varepsilon}_b + \boldsymbol{\Phi}\boldsymbol{\varepsilon}_\phi \tag{7a}$$

$$\tilde{\boldsymbol{\gamma}} = \boldsymbol{\gamma}^{(0)} + \boldsymbol{\phi}_{,3}\boldsymbol{\psi} \tag{8a}$$

For the kth layer of thickness $h_\alpha^{(k)}$, the following expressions hold for the refined zigzag functions, [86],

$$\begin{aligned} \phi_1^{(k)}(z) &= (z+\frac{h}{2})\left(\frac{G_4}{\bar{Q}_{44}^{(k)}(z)}-1\right)+\sum_{q=2}^{k} h^{(q-1)}\left(\frac{G_4}{\bar{Q}_{44}^{(q-1)}(z)}-\frac{G_4}{\bar{Q}_{44}^{(k)}(z)}\right) \\ \phi_2^{(k)}(z) &= (z+\frac{h}{2})\left(\frac{G_5}{\bar{Q}_{55}^{(k)}(z)}-1\right)+\sum_{q=2}^{k} h^{(q-1)}\left(\frac{G_5}{\bar{Q}_{55}^{(q-1)}(z)}-\frac{G_5}{\bar{Q}_{55}^{(k)}(z)}\right) \end{aligned} \quad (k=1,\dots,N) \tag{9}$$

where

$$G_j = \left(\frac{1}{h}\sum_{k=1}^{N}\int_{z_b^{(k)}}^{z_t^{(k)}}\frac{dz}{\bar{Q}_{jj}^{(k)}(z)}\right)^{-1} \qquad j=4,5 \tag{10}$$

and $\bar{Q}_{jj}^{(k)}(z)$ is the transformed transverse shear stiffness modulus of the kth layer (see Section 2.4).

It is noted that the *refined zigzag functions* $\phi_\alpha^{(k)}$ are piecewise continuous functions of the thickness co-ordinate and vanish on the bottom ($z=-h/2$) and top ($z=+h/2$) surfaces of the plate. They are *a priori* known, in that they depend only on the law of distribution of the transverse shear moduli of each layer, on the number of layers and on their thickness.

Note that, contrary to what happens for the traditional multilayered composite and sandwich structures where $\phi_\alpha^{(k)}$ is a piecewise linear function of the z-coordinate [104–108], for multilayered structures with layers made of functionally graded materials, $\phi_\alpha^{(k)}$ is a piecewise-non-linear function whose shape is regulated by the grading law of the transverse shear stiffness, [86]. Thus, the transverse shear strains $\gamma_{\alpha 3}^{(k)}$ are nonlinear functions of the thickness co-ordinate within each layer (see, Eq. 8a).

2.5 Stress-strain relations

The constitutive equations for a functionally graded layer are[2]

$$\begin{Bmatrix} \tilde{\sigma}_{11} \\ \tilde{\sigma}_{22} \\ \tilde{\sigma}_{12} \end{Bmatrix}^{(k)} = \begin{bmatrix} \bar{Q}_{11} & \bar{Q}_{12} & \bar{Q}_{16} \\ \bar{Q}_{12} & \bar{Q}_{22} & \bar{Q}_{26} \\ \bar{Q}_{16} & \bar{Q}_{26} & \bar{Q}_{66} \end{bmatrix}^{(k)} \begin{Bmatrix} \tilde{\varepsilon}_{11} \\ \tilde{\varepsilon}_{22} \\ \tilde{\gamma}_{12} \end{Bmatrix}^{(k)} \tag{11}$$

$$\begin{Bmatrix} \tilde{\sigma}_{13} \\ \tilde{\sigma}_{23} \end{Bmatrix}^{(k)} = \begin{bmatrix} \bar{Q}_{44} & \bar{Q}_{45} \\ \bar{Q}_{45} & \bar{Q}_{55} \end{bmatrix}^{(k)} \begin{Bmatrix} \tilde{\gamma}_{13} \\ \tilde{\gamma}_{23} \end{Bmatrix}^{(k)} \tag{12}$$

In compact matrix format,

$$\tilde{\boldsymbol{\sigma}}_p^{(k)} = \bar{\mathbf{Q}}_p^{(k)} \tilde{\boldsymbol{\varepsilon}}_p^{(k)} \tag{11a}$$

$$\tilde{\boldsymbol{\sigma}}_t^{(k)} = \bar{\mathbf{Q}}_t^{(k)} \tilde{\boldsymbol{\gamma}}^{(k)} \tag{12a}$$

where $\bar{Q}_{ij}^{(k)}(z)$ (i,j=1,2,6) and and $\bar{Q}_{ij}^{(k)}(z)$ (*i*,*j*=4,5) are the plane stress transformed stiffness moduli of the *k*th layer, that are functions of the z-coordinate.

2.6 Discrete equations of motion

The discretized equations of motion can be derived using the dynamic version of the principle of virtual displacements (D'Alembert principle)

$$\delta U - \delta W_{ext} = \delta W_{in} \tag{13}$$

where

$$\boldsymbol{\delta U} = \int_{-a/2}^{+a/2} \int_{-b/2}^{+b/2} \left\langle \delta \tilde{\boldsymbol{\varepsilon}}_p^T \tilde{\boldsymbol{\sigma}}_p + \delta \tilde{\boldsymbol{\gamma}}^T \tilde{\boldsymbol{\sigma}}_t \right\rangle dx_1 dx_2 \tag{14}$$

is the virtual variation of the work given by the internal forces (stress);

$$\delta W_{in} = -\int_{-a/2}^{+a/2} \int_{-b/2}^{+b/2} \left\langle \boldsymbol{\rho} \left(\ddot{\tilde{\mathbf{u}}}^T \delta \tilde{\mathbf{u}} + \ddot{\tilde{u}}_3 \delta \tilde{u}_3 \right) \right\rangle dx_1 dx_2 \tag{15}$$

is the virtual work of the inertia forces, and δW_{ex} is the virtual work of the applied forces,

$$\delta W_{ex} = 0 \tag{16}$$

for free vibration;

[2] In the present plate theory it is assumed $\sigma_{33} = 0$.

$$\delta W_{ex} = \int_{-a/2}^{+a/2}\int_{-b/2}^{+b/2} \bar{p}_3 \delta w dx_1 dx_2 + \\ + \int_{-a/2}^{+a/2} \bar{T}_{23}\left((x_1, -\frac{b}{2}, t)\delta w(x_1, -\frac{b}{2}, t) + (x_1, \frac{b}{2}, t)\delta w(x_1, \frac{b}{2}, t) \right) dx_1 + \\ + \int_{-b/2}^{+b/2}\left((-\frac{a}{2}, x_2, t)\delta w(-\frac{a}{2}, x_2, t) + \bar{T}_{13}(\frac{a}{2}, x_2, t)\delta w(\frac{a}{2}, x_2, t) \right) dx_2 \tag{17}$$

In writing Eq. (17) it is assumed that the plate is subjected to a transverse load $\bar{p}_3$ applied on the top surface of the plate, and to a boundary transverse loads per unit length $\bar{T}_{\alpha 3}$ $(\alpha = 1,2)$ applied on the edge parallel to x_α-axis.

In the previous equations, $\rho(x_3)$ is the material mass density; the overdot indicates differentiation with respect to the time, and an overbar the prescribed value of a quantity. All other symbols have been defined above. Moreover,

$$\langle \bullet \rangle = \sum_{s=1}^{N} \int_{x_3(s-1)}^{x_3(s)} (\bullet) dx_3$$

and δ is the variational operator.

Substitution of Eqs. (4)-(8) and (11) and (12) into Eqs. (14) and (15), yields

$$\delta U = \int_{-a/2}^{+a/2}\int_{-b/2}^{+b/2} \delta \mathbf{e}^T \mathbf{R} dx_1 dx_2 \tag{18}$$

where

$$\mathbf{R}^T = \left[\mathbf{N}^T \quad \mathbf{M}^T \quad \mathbf{M}_b^{(\phi)\mathrm{T}} \quad \mathbf{T}^T \quad \mathbf{T}^{(\phi)T} \right] \tag{19}$$

$$\mathbf{e}^T = \left[\boldsymbol{\varepsilon}_m^T \quad \boldsymbol{\varepsilon}_b^T \quad \boldsymbol{\varepsilon}_\phi^T \quad \boldsymbol{\gamma}^{(0)T} \quad \boldsymbol{\psi}^T \right] \tag{20}$$

In Eq. (19) the following force and moment stress resultants for unit length have been introduced

$$\left(\mathbf{N}, \mathbf{M}, \mathbf{M}_b^{(\phi)}\right) = \left(\begin{Bmatrix} N_{11} \\ N_{22} \\ N_{12} \end{Bmatrix}, \begin{Bmatrix} M_{11} \\ M_{22} \\ M_{12} \end{Bmatrix}, \begin{Bmatrix} M_{11}^{(\phi)} \\ M_{21}^{(\phi)} \\ M_{12}^{(\phi)} \\ M_{22}^{(\phi)} \end{Bmatrix} \right) = \left\langle \left(1, z, \begin{bmatrix} \phi_1^{(k)} & 0 & 0 \\ 0 & 0 & \phi_2^{(k)} \\ 0 & 0 & \phi_1^{(k)} \\ 0 & \phi_2^{(k)} & 0 \end{bmatrix} \right) \begin{Bmatrix} \tilde{\sigma}_{11} \\ \tilde{\sigma}_{22} \\ \tilde{\sigma}_{12} \end{Bmatrix} \right\rangle \tag{21}$$

$$\left(\mathbf{T}, \mathbf{T}^{(\phi)}\right) = \left(\begin{Bmatrix} T_1 \\ T_2 \end{Bmatrix}, \begin{Bmatrix} T_1^{(\phi)} \\ T_2^{(\phi)} \end{Bmatrix} \right) = \left\langle 1, \begin{bmatrix} \phi_{1,3}^{(k)} & 0 \\ 0 & \phi_{2,3}^{(k)} \end{bmatrix} \begin{Bmatrix} \tilde{\sigma}_{13} \\ \tilde{\sigma}_{23} \end{Bmatrix} \right\rangle \tag{22}$$

The **plate constitutive relations** are derived by using Eqs. (7) and (8) with Eqs. (10) and (11) into Eqs. (21) and (22), and integrating over the plate thickness. In matrix format they read

$$\mathbf{R} = \mathbf{S}\mathbf{e} \tag{23}$$

where

$$\mathbf{S} = \begin{bmatrix} \mathbf{A} & \mathbf{B} & \mathbf{A}_\phi & \mathbf{0} & \mathbf{0} \\ \mathbf{B} & \mathbf{D} & \mathbf{B}_\phi & \mathbf{0} & \mathbf{0} \\ \mathbf{A}_\phi^T & \mathbf{B}_\phi^T & \mathbf{D}_\phi & \mathbf{0} & \mathbf{0} \\ \mathbf{0} & \mathbf{0} & \mathbf{0} & \mathbf{A}_t & \mathbf{B}_t^\phi \\ \mathbf{0} & \mathbf{0} & \mathbf{0} & \mathbf{B}_t^{\phi T} & \mathbf{D}_t^\phi \end{bmatrix} \tag{24}$$

$$\begin{aligned} &\left(\mathbf{A},\mathbf{B},\mathbf{D}\right) = \left\langle (1,z,z^2)\bar{\mathbf{Q}}_p \right\rangle,\ \left(\mathbf{A}_\phi,\mathbf{B}_\phi,\mathbf{D}_\phi\right) = \left\langle \left(1,z,\mathbf{\Phi}^T\right)\bar{\mathbf{Q}}_p\mathbf{\Phi} \right\rangle \\ &\left(\mathbf{A}_t,\mathbf{B}_t\right) = \left\langle \bar{\mathbf{Q}}_t\left(1,\boldsymbol{\phi}_{,3}^{(k)}\right) \right\rangle,\ \mathbf{D}_t = \left\langle \boldsymbol{\phi}_{,3}^{(k)\mathrm{T}}\mathbf{Q}_t\boldsymbol{\phi}_{,3}^{(k)} \right\rangle \end{aligned} \tag{25}$$

For the virtual work of inertia forces, we obtain

$$\begin{aligned} \delta W_{in} &= -\int_{-a/2}^{+a/2}\int_{-b/2}^{+b/2} \left\langle \rho\delta\tilde{u}_i^T\ddot{\tilde{u}}_i \right\rangle dx_1dx_2 = -\int_{-a/2}^{+a/2}\int_{-b/2}^{+b/2} \left\langle \rho\left(\delta\tilde{\mathbf{u}}^T\ddot{\tilde{\mathbf{u}}} + \delta\tilde{u}_3\ddot{\tilde{u}}_3\right)\right\rangle dx_1dx_2 \\ &= -\int_{-a/2}^{+a/2}\int_{-b/2}^{+b/2} \delta\mathbf{d}^T\mathbf{m}\ddot{\mathbf{d}}\ dx_1dx_2 \end{aligned} \tag{26}$$

where

$$\mathbf{d} = \begin{Bmatrix} u_1 \\ u_2 \\ \theta_1 \\ \theta_2 \\ \psi_1 \\ \psi_2 \\ w \end{Bmatrix};\ \ \mathbf{m} = \begin{bmatrix} m^{(0)} & 0 & m^{(1)} & 0 & m_1^{(0)} & 0 & 0 \\ 0 & m^{(0)} & 0 & m^{(1)} & 0 & m_2^{(0)} & 0 \\ m^{(1)} & 0 & m^{(2)} & 0 & m_1^{(1)} & 0 & 0 \\ 0 & m^{(1)} & 0 & m^{(2)} & 0 & m_2^{(1)} & 0 \\ m_1^{(0)} & 0 & m_1^{(1)} & 0 & m_1^{(2)} & 0 & 0 \\ 0 & m_1^{(0)} & 0 & m_2^{(1)} & 0 & m_2^{(2)} & 0 \\ 0 & 0 & 0 & 0 & 0 & 0 & m^{(0)} \end{bmatrix} \tag{27}$$

$$\left(m^{(0)},m^{(1)},m^{(2)},m_\alpha^{(0)},m_\alpha^{(1)},m_\alpha^{(2)}\right) = \left\langle \rho\left(1,z,z^2,\phi_\alpha^{(k)},z\phi_\alpha^{(k)},z\phi_\alpha^{(k)2}\right)\right\rangle \tag{28}$$

Due to difficulty to obtain closed form solutions, we search for an approximate solution transforming the differential problem in an algebraic problem. In order to do this, in the following the discretization is accomplished directly in the D'Alembert principle previously stated using the Ritz method [102, 103].

Let us expand the unknown functions in the form,

$$\hat{f}\left(\xi_1,\xi_2,t\right) = \sum_{m=1}^{M(f)} C_m^{(f)}(t)g_m^{(f)}\left(\xi_1,\xi_2\right) = \mathbf{g}^{(f)T}\mathbf{C}^{(f)} \tag{29}$$

where $\hat{f}(\xi_1,\xi_2,t)$ stands for $\hat{u}_\alpha(\xi_1,\xi_2,t)$, $\hat{w}(\xi_1,\xi_2,t)$, $\hat{\theta}_\alpha(\xi_1,\xi_2,t)$ and $\hat{\psi}_\alpha(\xi_1,\xi_2,t)$ ($\alpha=1,2$), respectively. In Eq. (29), $C_m^{(f)}(t)$ are unknown coefficients (generalized coordinates) to be varied, and $g_m^{(f)}(\xi_1,\xi_2)$ are the approximating functions. In the Ritz method, these functions are required to be a complete set at least linearly independent and satisfying the geometric (prescribed, kinematic) boundary conditions (these functions are named admissible functions in the literature).

Appendix A gives details of the admissible functions used in this work.

Thus, by taking into account Eqs. (7), (8) and (20)

$$\mathbf{d}=\begin{Bmatrix} u_1\\ u_2\\ \theta_1\\ \theta_2\\ \psi_1\\ \psi_2\\ w \end{Bmatrix}=\begin{bmatrix} \mathbf{g}^{u_1T} & \mathbf{0} & \mathbf{0} & \mathbf{0} & \mathbf{0} & \mathbf{0} & \mathbf{0}\\ \mathbf{0} & \mathbf{g}^{u_2T} & \mathbf{0} & \mathbf{0} & \mathbf{0} & \mathbf{0} & \mathbf{0}\\ \mathbf{0} & \mathbf{0} & \mathbf{g}^{\theta_1T} & \mathbf{0} & \mathbf{0} & \mathbf{0} & \mathbf{0}\\ 0 & \mathbf{0} & 0 & \mathbf{g}^{\theta_2T} & 0 & \mathbf{0} & 0\\ \mathbf{0} & 0 & \mathbf{0} & 0 & \mathbf{g}^{\psi_1T} & 0 & 0\\ 0 & \mathbf{0} & 0 & \mathbf{0} & 0 & \mathbf{g}^{\psi_2T} & 0\\ 0 & 0 & 0 & \mathbf{0} & 0 & 0 & \mathbf{g}^{wT} \end{bmatrix}\begin{Bmatrix} \mathbf{C}_{u_1}\\ \mathbf{C}_{u_2}\\ \mathbf{C}_{\theta_1}\\ \mathbf{C}_{\theta_2}\\ \mathbf{C}_{\psi_1}\\ \mathbf{C}_{\psi_2}\\ \mathbf{C}_{w} \end{Bmatrix} \tag{30}$$

$$\mathbf{e}=\begin{Bmatrix} \hat{\boldsymbol{\varepsilon}}_m\\ \hat{\boldsymbol{\varepsilon}}_b\\ \hat{\boldsymbol{\varepsilon}}_\phi\\ \hat{\boldsymbol{\gamma}}^{(0)}\\ \boldsymbol{\psi} \end{Bmatrix}=\begin{bmatrix} \mathbf{g}_{,1}^{u_1T} & \mathbf{0} & \mathbf{0} & \mathbf{0} & \mathbf{0} & \mathbf{0} & \mathbf{0}\\ \mathbf{0} & \mathbf{g}_{,2}^{u_2T} & \mathbf{0} & \mathbf{0} & \mathbf{0} & \mathbf{0} & \mathbf{0}\\ \mathbf{g}_{,2}^{u_2T} & \mathbf{g}_{,1}^{u_1T} & \mathbf{0} & \mathbf{0} & \mathbf{0} & \mathbf{0} & \mathbf{0}\\ \mathbf{0} & \mathbf{0} & \mathbf{g}_{,1}^{\theta_1T} & \mathbf{0} & \mathbf{0} & \mathbf{0} & \mathbf{0}\\ \mathbf{0} & \mathbf{0} & \mathbf{0} & \mathbf{g}_{,2}^{\theta_2T} & \mathbf{0} & \mathbf{0} & \mathbf{0}\\ \mathbf{0} & \mathbf{0} & \mathbf{g}_{,2}^{\theta_1T} & \mathbf{g}_{,1}^{\theta_2T} & \mathbf{0} & \mathbf{0} & \mathbf{0}\\ \mathbf{0} & \mathbf{0} & \mathbf{0} & \mathbf{0} & \mathbf{g}_{,1}^{\psi_1T} & \mathbf{0} & \mathbf{0}\\ \mathbf{0} & \mathbf{0} & \mathbf{0} & \mathbf{0} & \mathbf{0} & \mathbf{g}_{,1}^{\psi_2T} & \mathbf{0}\\ \mathbf{0} & \mathbf{0} & \mathbf{0} & \mathbf{0} & \mathbf{g}_{,2}^{\psi_1T} & \mathbf{0} & \mathbf{0}\\ \mathbf{0} & \mathbf{0} & \mathbf{0} & \mathbf{0} & \mathbf{0} & \mathbf{g}_{,2}^{\psi_2T} & \mathbf{0}\\ \mathbf{0} & \mathbf{0} & \mathbf{g}_{,1}^{\theta_1T} & \mathbf{0} & \mathbf{0} & \mathbf{0} & \mathbf{g}_{,1}^{wT}\\ \mathbf{0} & \mathbf{0} & \mathbf{0} & \mathbf{g}_{,2}^{\theta_2T} & \mathbf{0} & \mathbf{0} & \mathbf{g}_{,2}^{wT}\\ \mathbf{0} & \mathbf{0} & \mathbf{0} & \mathbf{0} & \mathbf{g}_{,1}^{\psi_1T} & \mathbf{0} & \mathbf{0}\\ \mathbf{0} & \mathbf{0} & \mathbf{0} & \mathbf{0} & \mathbf{0} & \mathbf{g}_{,1}^{\psi_2T} & \mathbf{0} \end{bmatrix}\begin{Bmatrix} \mathbf{C}_{u_1}\\ \mathbf{C}_{u_2}\\ \mathbf{C}_{\theta_1}\\ \mathbf{C}_{\theta_2}\\ \mathbf{C}_{\psi_1}\\ \mathbf{C}_{\psi_2}\\ \mathbf{C}_{w} \end{Bmatrix} \tag{31}$$

In compact matrix format,

$$\mathbf{d}=\mathbf{G}\mathbf{C} \tag{30a}$$

$$\mathbf{e}=\mathbf{G}_\nabla\mathbf{C} \tag{31a}$$

Substituting this relation into Eqs. (18), (26) and (16), yields

$$\delta U = \delta \mathbf{C}^T \int_{-a/2}^{+a/2} \int_{-b/2}^{+b/2} \left(\mathbf{G}_\Delta^T \begin{bmatrix} \mathbf{A} & \mathbf{B} & \mathbf{A}^\phi & \mathbf{0} & \mathbf{0} \\ \mathbf{B} & \mathbf{D} & \mathbf{B}^\phi & \mathbf{0} & \mathbf{0} \\ \mathbf{A}^{\phi T} & \mathbf{B}^{\phi T} & \mathbf{D}^\phi & \mathbf{0} & \mathbf{0} \\ \mathbf{0} & \mathbf{0} & \mathbf{0} & \mathbf{A}_t & \mathbf{B}_t^\phi \\ \mathbf{0} & \mathbf{0} & \mathbf{0} & \mathbf{B}_t^{\phi T} & \mathbf{D}_t^\phi \end{bmatrix} \mathbf{G}_\Delta dx_1 dx_2 \right) = \delta \mathbf{C}^T \mathbf{K} \mathbf{C} \tag{32}$$

$$\delta W_{in} = -\delta \mathbf{C}^T \left(\int_{-a/2}^{+a/2} \int_{-b/2}^{+b/2} \mathbf{G}^T \mathbf{m} \mathbf{G} dx_1 dx_2 \right) \ddot{\mathbf{C}} = -\delta \mathbf{C}^T \mathbf{M} \ddot{\mathbf{C}} \tag{33}$$

with

$$\mathbf{K} = \int_{-a/2}^{+a/2} \int_{-b/2}^{+b/2} \mathbf{G}_\Delta^T \begin{bmatrix} \mathbf{A} & \mathbf{B} & \mathbf{A}^\phi & \mathbf{0} & \mathbf{0} \\ \mathbf{B} & \mathbf{D} & \mathbf{B}^\phi & \mathbf{0} & \mathbf{0} \\ \mathbf{A}^{\phi T} & \mathbf{B}^{\phi T} & \mathbf{D}^\phi & \mathbf{0} & \mathbf{0} \\ \mathbf{0} & \mathbf{0} & \mathbf{0} & \mathbf{A}_t & \mathbf{B}_t^\phi \\ \mathbf{0} & \mathbf{0} & \mathbf{0} & \mathbf{B}_t^{\phi T} & \mathbf{D}_t^\phi \end{bmatrix} \mathbf{G}_\Delta dx_1 dx_2 \tag{34}$$

$$\mathbf{M} = \int_{-a/2}^{+a/2} \int_{-b/2}^{+b/2} \mathbf{G}^T \mathbf{m} \mathbf{G} dx_1 dx_2 \tag{35}$$

$$\delta W_{ex} = \delta \mathbf{C}^T \mathbf{P} \tag{36}$$

where

$$\mathbf{P} = \mathbf{0} \tag{37}$$

for free vibration;

$$\mathbf{P}^T = \int_{-a/2}^{+a/2} \int_{-b/2}^{+b/2} \lfloor 0 \quad 0 \quad 0 \quad 0 \quad 0 \quad 0 \quad \bar{p}_3 \rfloor \mathbf{G} dx_1 dx_2 + \int_{\Gamma_p} \lfloor 0 \quad 0 \quad 0 \quad 0 \quad 0 \quad 0 \quad \bar{T}_3 \rfloor \mathbf{G} d\Gamma \tag{38}$$

and

$$\begin{aligned} \int_{\Gamma_p} \bar{T}_3 \, \mathbf{G} d\Gamma &= \int_{-a/2}^{+a/2} \left(\bar{T}_{23}(x_1, -\frac{b}{2}) \mathbf{g}^w(x_1, -\frac{b}{2}) + \bar{T}_{23}(x_1, \frac{b}{2}) \mathbf{g}^w(x_1, \frac{b}{2}) \right) dx_1 + \\ &+ \int_{-b/2}^{+b/2} \left(\bar{T}_{13}(-\frac{a}{2}, x_2) \mathbf{g}^w(-\frac{a}{2}, x_2) + \bar{T}_{13}(\frac{a}{2}, x_2) \mathbf{g}^w(\frac{a}{2}, x_2) \right) dx_2 \\ &= \frac{a}{2} \int_{-1}^{+1} \left(\bar{T}_{23}(\xi, -1) \mathbf{g}^w(\xi, -1) + \bar{T}_{23}(\xi, 1) \mathbf{g}^w(\xi, 1) \right) d\xi + \\ &+ \frac{b}{2} \int_{-1}^{+1} \left(\bar{T}_{13}(-1, \eta) \mathbf{g}^w(-1, \eta) + \bar{T}_{13}(1, \eta) \mathbf{g}^w(1, \eta) \right) d\eta \end{aligned} \tag{39}$$

Substitution of Eqs. (32), (33) and (36) into Eq. (13), taking into account that the virtual variation are arbitrary independent variations yields the following approximate discretized ***equations of motion***

$$\mathbf{M} \ddot{\mathbf{C}} + \mathbf{K} \mathbf{C} = \mathbf{P} \tag{40}$$

3 Numerical results and discussion

In this Section, numerical results on bending and free vibration of different functionally graded plates are presented.

First, to assess the capabilities of the proposed Refined Zigzag Theory in conjunction with the Ritz method with orthogonal polynomials in predicting both global (i.e., deflection, natural frequencies and mode shapes) and local (i.e., through-the-thickness distribution of in-plane displacements and stresses) responses of functionally graded plates with Ceramic/Metal phases and sandwich plates under various boundary conditions, are considered. All the results of transverse shear stresses are computed by integration of the local three-dimensional equilibrium equations. Two types of plates are taken into consideration (see Figure 2): a monolayer functionally graded plate (Figure 2-a) and a sandwich plate with functionally graded face-sheet and homogeneous core (Figure 2-b).

Mechanical material properties for monolayer and sandwich plate are listed in Table 2. The materials indicated in Table 2 are for the most isotropic, except only one, called "orthotropic", has the mechanical properties different along the principal directions. The stacking sequence for the various plate considered later are exposed in Table 3. In column "Lamina Materials" of Table 3 the abbreviation of FG indicates that the layer considered is a functionally graded layer with the materials shown by the letters in brackets.

Table 2. Mechanical properties of isotropic and orthotropic materials used.

Material	$E_1\ [GPa]$	$E_2\ [GPa]$	$E_3\ [GPa]$	ν_{12}	ν_{13}	ν_{23}	$G_{12}\ [GPa]$	$G_{13}\ [GPa]$	$G_{23}\ [GPa]$	$\rho\ \left[\frac{kg}{m^3}\right]$
Al (A1)	70	70	70	0.3	0.3	0.3	26.923	26.923	26.923	2707
Al (A2)	70	70	70	0.3	0.3	0.3	26.923	26.923	26.923	2702
Al_2O_3 (B)	380	380	380	0.3	0.3	0.3	146.154	146.154	146.154	3800
ZrO_2 (C)	200	200	200	0.3	0.3	0.3	76.92	76.92	76.92	5700
Orthotropic (O)	174.6	6.89	6.89	0.25	0.25	0.25	3.5	3.5	1.4	1000

Table 3. Laminate stacking sequences (from bottom to top surface) for monolayer and sandwich plate.

Laminate	Normalized lamina thickness $h^{(k)}/h$	Lamina Materials	Lamina Orientation [°]
L1	(0.3333/0.3333/0.3333)	FG (O)/O/FG (O)	(0/Core/0)
L2	Monolayer	FG (A2/B)	(0)
L3	(0.25/0.5/0.25)	FG (A1/B)/B/FG(B/A1)	(0/Core/0)
L4	(0.25/0.5/0.25)	FG(B/A1)/A1/FG(A1/B)	(0/Core/0)
L5	(0.25/0.5/0.25)	FG (O)/O/FG(O)	(0/Core/0)
L6	Monolayer	FG (A2/C)	(0)
L7	Variable (see, Table 13)	FG(B/A1)/A1/FG(A1/B)	(0/Core/0)

For the assessment, 3D and 2D analytical and FEM results are used.

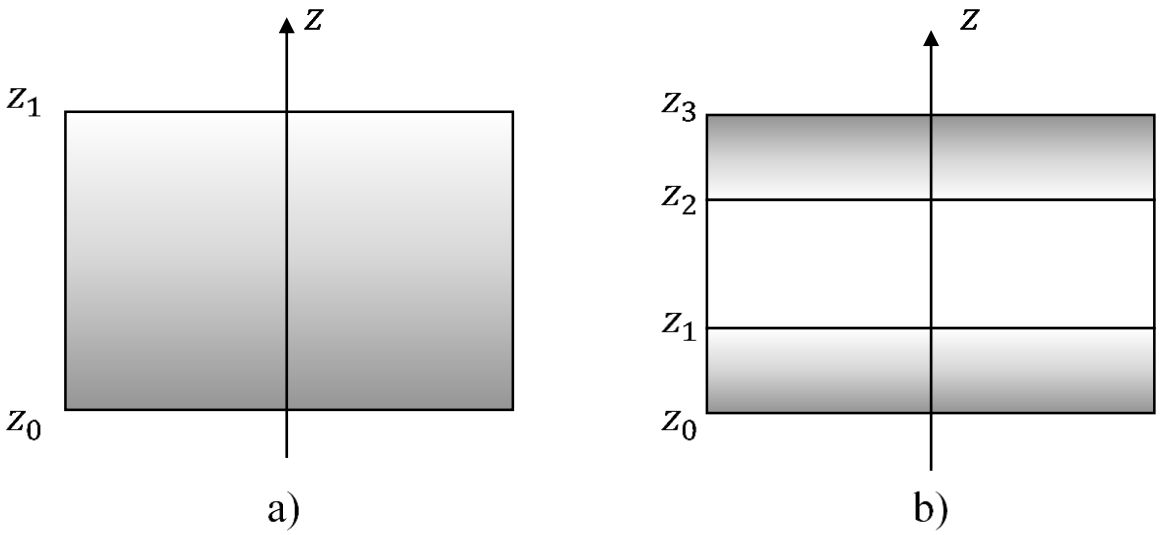

Fig. 2. Configuration of functionally graded plates: (a) functionally graded monolayer plate; (b) sandwich plate with functionally graded face-sheets and homogeneous core.

3.1 Convergence study

In order to assess the accuracy of the RZT and the convergence characteristics of the Ritz method using orthogonal polynomials, a simply supported sandwich square plate with functionally graded face-sheet (L1) (Figure 2-b), under bi-sinusoidal pressure is considered. According to Iurlaro et al [86], the assumed exponential (E-FGM) grading law for the mechanical properties (Young moduli, shear moduli and mass density) of orthotropic material (Table 2, material O) is, in this example, $ln\frac{P_t^{(3)}}{P_b^{(3)}} = 5$ (see, Table 1). As the effective Poisson's ratio depends weakly on position, in this study it is assumed constant along the thickness.

The convergence results for increasing number of the orthogonal polynomials (N_1 in the x_1-direction and N_2 in the x_2-direction) for simply supported sandwich square plate (L1) are given in Table 4. In Table 4, and in the following body of paper, the non-dimensional quantities are defined as:

$$\bar{u}_1 = 10^3 \frac{h^2 E_2 u_1}{q_0 a^3} \qquad \bar{u}_3 = 10^3 \frac{h^2 E_2 u_3}{q_0 a^3}$$
$$\left(\bar{\sigma}_{11}, \bar{\sigma}_{22}, \bar{\tau}_{12}\right) = \frac{h^2}{q_0 a^2}\left(\sigma_{11}, \sigma_{22}, \tau_{12}\right) \qquad \left(\bar{\tau}_{13}, \bar{\tau}_{23}\right) = \frac{h}{q_0 a}\left(\tau_{13}, \tau_{23}\right) \tag{41}$$

Table 4. Convergence results for bending of simply supported sandwich square plate (L1), $\ln\frac{P_t}{P_b}=5$ and *a/h*=8 under bi-sinusoidal transverse load. For non-dimensional quantities $E_2=E_{2_{core}}$.

	$\bar{u}_3(0,0)$	$\bar{u}_1\left(-\frac{a}{2},0,\frac{h}{2}\right)$	$\bar{\sigma}_{11}\left(0,0,\frac{h}{2}\right)$	$\bar{\sigma}_{22}\left(0,0,\frac{h}{2}\right)$	$\bar{\tau}_{12}\left(-\frac{a}{2},-\frac{b}{2},\frac{h}{2}\right)$	$\bar{\tau}_{13}\left(-\frac{a}{2},0,0\right)$	$\bar{\tau}_{23}\left(0,-\frac{b}{2},0\right)$
3D solution	9.685	-0.3093	3.652	0.3343	-0.221	0.2116	0.0687
RZT [86]	9.6344	-0.3034	3.5428	0.3344	-0.2215	0.2101	0.0680
RZT							
$N_1=N_2$	$\bar{u}_3(0,0)$	$\bar{u}_1\left(-\frac{a}{2},0,\frac{h}{2}\right)$	$\bar{\sigma}_{11}\left(0,0,\frac{h}{2}\right)$	$\bar{\sigma}_{22}\left(0,0,\frac{h}{2}\right)$	$\bar{\tau}_{12}\left(-\frac{a}{2},-\frac{b}{2},\frac{h}{2}\right)$	$\bar{\tau}_{13}\left(-\frac{a}{2},0,0\right)$	$\bar{\tau}_{23}\left(0,-\frac{b}{2},0\right)$
1	0.8233	0	0	0	0	0	0
2	8.4835	-0.3253	2.444	0.2277	-0.3025	0.02874	0.0214
3	8.5564	-0.3296	2.476	0.2326	-0.2714	0.02536	0.0244
4	9.6025	-0.3028	3.51	0.3315	-0.2219	0.2633	0.0805
5	9.6041	-0.303	3.512	0.3317	-0.2234	0.2641	0.0809
6	9.6336	-0.3033	3.579	0.3378	-0.2239	0.2071	0.0673
7	9.6336	-0.3033	3.579	0.3378	-0.2238	0.2071	0.0673
8	9.6339	-0.3033	3.58	0.338	-0.2238	0.2102	0.0680
9	9.6339	-0.3033	3.58	0.338	-0.2238	0.2102	0.0680

Results in Table 4 are compared with RZT analytical solutions obtained by Iurlaro et al [86] and 3D solution using Pagano approach [123]. It is concluded that there is a good agreement between two results. It is observed that using 8 orthogonal polynomials in both the directions guarantees the convergence of the Ritz results to the correct results for both global and local values of displacements and stresses.

To show the convergence of the Ritz method for free vibration problem, in Table 5 the first eight non-dimensional frequencies $\left(\bar{f}=\frac{\omega a^2}{2\pi h}\sqrt{\frac{\rho_{core}}{E_{2_{core}}}}\right)$ of the same sandwich plate clamped on the side $x_1=-\frac{a}{2}$ and free on the other sides are presented for increasing number of orthogonal polynomials.

Table 5. Convergence analysis for free vibration problem of cantilevered sandwich square plate (L1), $\ln \frac{P_t}{P_b} = 5$ and *a*/*h*=8.

RZT								
$N_1 = N_2$	1	2	3	4	5	6	7	8
1	0.8715	-	-	-	-	-	-	-
2	0.5749	0.6510	-	-	-	-	-	-
3	0.4785	0.5542	1.2070	1.3944	2.0575	2.1374	2.4694	3.3969
4	0.4667	0.5351	1.1745	1.3578	1.6423	1.7198	2.0429	2.0941
5	0.4663	0.5345	1.0473	1.3570	1.6184	1.6955	1.9625	2.0109
6	0.4662	0.5336	1.0450	1.3477	1.6163	1.6450	1.6988	1.9594
7	0.4662	0.5336	1.0367	1.3476	1.6163	1.6387	1.6981	1.9515
8	0.4662	0.5334	1.0366	1.3452	1.6052	1.6162	1.6961	1.9514
9	0.4662	0.5334	1.0365	1.3451	1.6051	1.6162	1.6961	1.9511
3D (FEM) [86]	0.465	0.531	1.034	1.345	1.593	1.598	1.673	1.926

It is concluded that a good approximation for the first eight frequencies is obtained with 9 orthogonal polynomials.

Unless otherwise specified, it is understood that the numerical results presented below were obtained using the Ritz method with 8 orthogonal polynomials in the x_1 and x_2 directions. Furthermore, if not explicitly stated, the acronym TSDT is used to indicate numerical results obtained using Reddy third-order shear deformation theory [124] and 3D those obtained using 3D Pagano exact solution [123].

3.2 Bending problem

In this first analysis, a simply supported square plate Ceramic/Metal (L2) with span-to-thickness ratio $(a/h = 10)$ under bi-sinusoidal transverse pressure is considered. The grading law for mechanical properties is the power law (see, Table 1); two values of the grading index are considered: *p*=0.2 and 1.

Table 6 gives the non-dimensional transverse displacement and the non-dimensional in-plane and transverse shear stresses computed using different theories (CPT, FSDT, TSDT, RZT). For comparison, 3D results obtained using Pagano exact solution [123] and those obtained by Redddy et al. [73] using Higher-Order Shear Deformation Theory are shown. For *p*=1, results obtained by Thai et al [84] are also quoted.

As known, in order to obtain more accurate results, FSDT need the use of shear correction factors. In this study, in addition to the classical ones $(k_1^2 = k_2^2 = 1; \frac{5}{6}; \frac{2}{3}; \frac{\pi^2}{12})$, also ad hoc computed shear correction factors, Raman et al [125] have been used.

Table 6. Comparison of non-dimensional displacement and stresses for simply supported square (L2) FG Ceramic/Metal plate (a/h= 10). In the non-dimensional quantities $E_c = E_2$ of ceramic phase.

p	Theory		$\bar{u}_3(0,0,0)$	$\bar{\sigma}_{11}\left(0,0,\frac{h}{2}\right)$	$\bar{\sigma}_{22}\left(0,0,\frac{h}{3}\right)$	$\bar{\tau}_{12}\left(-\frac{a}{2},-\frac{b}{2},-\frac{h}{3}\right)$	$\bar{\tau}_{13}\left(-\frac{a}{2},0,0\right)$	$\bar{\tau}_{23}\left(0,-\frac{b}{2},\frac{h}{6}\right)$
0.2	CPT		341.6178	0.2235	0.1393	0.07211	0.2426	0.2255
	FSDT	$k_1^2 = k_2^2 = 1$	356.8597	0.2235	0.1393	0.07211	0.2426	0.2255
		$k_1^2 = k_2^2 = \frac{5}{6}$	359.9081	0.2235	0.1393	0.07211	0.2426	0.2255
		$k_1^2 = k_2^2 = \frac{2}{3}$	364.4807	0.2235	0.1393	0.07211	0.2426	0.2255
		$k_1^2 = k_2^2 = \frac{\pi^2}{12}$	360.1498	0.2235	0.1393	0.07211	0.2426	0.2255
		$k_1^2 = 0.84375$ $k_2^2 = 0.84375$	359.6823	0.2235	0.1393	0.07211	0.2426	0.2255
	TSDT		359.6707	0.2256	0.1388	0.07192	0.2421	0.2253
	Redddy et al [73]		359.9	0.2259	0.1387	0.07206	0.2423	0.2254
	RZT		357.0589	0.2231	0.1392	0.07214	0.2426	0.2253
	3D		357.9103	0.2266	0.1404	0.07206	0.2422	0.2254
1	CPT		562.2550	0.3041	0.1500	0.06101	0.2388	0.2509
	FSDT	$k_1^2 = k_2^2 = 1$	584.5006	0.3041	0.1500	0.06101	0.2388	0.2509
		$k_1^2 = k_2^2 = \frac{5}{6}$	588.9498	0.3041	0.1500	0.06101	0.2388	0.2509
		$k_1^2 = k_2^2 = \frac{2}{3}$	595.6235	0.3041	0.1500	0.06101	0.2388	0.2509
		$k_1^2 = k_2^2 = \frac{\pi^2}{12}$	589.3025	0.3041	0.1500	0.06101	0.2388	0.2509
		$k_1^2 = 0.8304$ $k_2^2 = 0.8304$	589.0446	0.3041	0.1500	0.06101	0.2388	0.2509
	TSDT		588.9317	0.3072	0.1493	0.06088	0.2382	0.2507
	Redddy et al [73]		589.0	0.3088	0.1490	0.06107	0.2384	0.2547
	Thai et al [84]		588.9	0.3087	0.1489	0.06110	0.2462	0.2622
	RZT		584.6298	0.3044	0.1501	0.06092	0.2388	0.2509
	3D		587.5220	0.3085	0.1510	0.06089	0.2383	0.2509

Results collected in Table 6 show that in this case classical plate theory (CPT) and first-order shear deformation plate theory (FSDT) with various shear correction factors, produce for the non-dimensional stresses indistinguishable results. Similar conclusions are reached by Reddy [47]. In general, with respect to Pagano solution, these theories under-estimate the central displacement. The effect of transverse shear is more evident considering Reddy third-order shear deformation plate theory (TSDT) and RZT. Both theories for this problem are capable of predict, with a good accuracy, the local behavior. The maximum transverse displacement for $p = 0.2$ computed using the RZT is closer to the 3D solution than those computed using TSDT: there is 0.5% of difference between TSDT and the 3D solution and only the 0.224% of difference between the 3D solution and RZT. The RZT results for the transverse displacement are more accurate than those obtained in Ref. [73] using third-order shear deformation plate theory. The authors consider a cubic

kinematics for in-plane displacements and constant transverse displacement in the thickness-wise direction, thus the adopted model has 9 unknown generalized displacements, while RZT has only 7 unknown generalized displacements. In general, considering the distribution through the thickness of in-plane displacement and stresses, for a P-FGM with p=0.2 and 1 there is not evident difference between the predictions of various theories.

Now, we consider a simply supported sandwich square plate (L3) with Ceramic/Metal P-FGM face-sheets under bi-sinusoidal pressure. Results for non-dimensional in-plane and transverse displacements and in-plane and transverse shear stresses considering different theories and different span-to-thickness ratios are collected in Table 7. In this case, for comparison purpose, the non-dimensional displacements are taken:

$$\bar{u} = 10^3 \frac{h^2 E_{core} u}{q_0 a^3} \qquad \bar{w} = 10^3 \frac{h^3 E_{core} w}{q_0 a^4} \tag{42}$$

The exponent used for the power law is $p = 0.5$ The present results are also compared with those obtained by Natarajan et al. [83] using FEM based on FSDT (FSDT5 results) and zig-zag TSDT (HSDT13 results) theories.

From Table 7 we observe that for thin plate (a/h=100) all theories considered (CPT, FSDT using Raman's shear correction factors, Reddy TSDT and RZT) produce the same results of Pagano 3D solution. For thick and moderately thick sandwich plates, the RZT results are closer than those computed with other theories. Although the RZT is, as said, the best theory (in the sense that it represents the best compromise between accuracy and computational cost) to study the behavior of thick plates, it is also very well indicated to study thin plates, producing the same results of the CPT. The RZT results are also very close to 3D Pagano solution than those obtained by Natarajan et al [83] using a FEM solution based on FSDT and HSDT.

In Figure 3 are plotted the thickness-wise distributions of non-dimensional in-plane and transverse displacements and non-dimensional in-plane and transverse shear stresses for a simply supported sandwich plate (L4) with P-FGM face-sheet (with power law exponent $p = 10$) under bi-sinusoidal transverse pressure. The core-to-face thickness ratio $h_c/h_f = 2$ and the span to thickness ratio a/h=5 (thick plate). To assess the present formulation, Table 8 shows the most relevant values from Figure 3 computed with the RZT with the results present in literature, Nguyen et al [76], where the author considered a refined higher-order hyperbolic shear deformation theory. The non-dimensional values of the displacements given by (41) are computed using the Young modulus of ceramic phase.

Table 7. Comparison of local and global behavior for a simply supported sandwich square plate (L3) with P-FGM face-sheets (p=0.5) under bi-sinusoidal pressure. Core-to-face thickness ratio $\frac{h_c}{h_f} = 2$.

a/h	Theory		$\bar{u}_3(0,0)$	$\bar{u}_1\left(-\frac{a}{2},0,-\frac{h}{2}\right)$	$\bar{\sigma}_{11}\left(0,0,-\frac{h}{2}\right)$	$\bar{\tau}_{12}\left(-\frac{a}{2},-\frac{b}{2},-\frac{h}{2}\right)$	$\bar{\tau}_{13}\left(-\frac{a}{2},0,0\right)$
5	CPT		40.0382	62.8919	-0.0683	0.0368	0.2623
	FSDT	$k_1^2 = k_2^2 = 1$	46.1359	62.8919	-0.0683	0.0368	0.2623
		$k_1^2 = k_2^2 = \frac{5}{6}$	47.3554	62.8919	-0.0683	0.0368	0.2623
		$k_1^2 = k_2^2 = \frac{2}{3}$	49.1847	62.8919	-0.0683	0.0368	0.2623
		$k_1^2 = k_2^2 = \frac{\pi^2}{12}$	47.4521	62.8919	-0.0683	0.0368	0.2623
		$k_1^2 = 0.8793$ $k_2^2 = 0.8793$	46.9727	62.8919	-0.0683	0.0368	0.2623
	TSDT		46.9524	64.9883	-0.0706	0.0380	0.2605
	FSDT5 [83]		47.3860	62.9280	-0.0527	0.0284	0.2616
	HSDT13 [83]		44.0040	63.7260	-0.0547	0.0287	0.2601
	RZT		46.6627	64.5437	-0.0701	0.0377	0.2617
	3D		45.8241	63.7018	-0.0692	0.0372	0.2602
10	CPT		40.0382	62.8919	-0.0683	0.0368	0.2623
	FSDT	$k_1^2 = k_2^2 = 1$	41.5626	62.8919	-0.0683	0.0368	0.2623
		$k_1^2 = k_2^2 = \frac{5}{6}$	41.8675	62.8919	-0.0683	0.0368	0.2623
		$k_1^2 = k_2^2 = \frac{2}{3}$	42.3248	62.8919	-0.0683	0.0368	0.2623
		$k_1^2 = k_2^2 = \frac{\pi^2}{12}$	41.8917	62.8919	-0.0683	0.0368	0.2623
		$k_1^2 = 0.8793$ $k_2^2 = 0.8793$	41.7719	62.8919	-0.0683	0.0368	0.2623
	TSDT		41.7692	63.4168	-0.0689	0.0371	0.2618
	FSDT5 [83]		41.8760	62.9280	-0.0527	0.0284	0.2616
	HSDT13 [83]		41.0780	63.1560	-0.0532	0.0285	0.2615
	RZT		41.6949	63.3065	-0.0687	0.0370	0.2621
	3D		41.4913	63.1219	-0.0685	0.0369	0.2617
100	CPT		40.0382	62.8919	-0.0683	0.0368	0.2623
	FSDT	$k_1^2 = k_2^2 = 1$	40.0535	62.8919	-0.0683	0.0368	0.2623
		$k_1^2 = k_2^2 = \frac{5}{6}$	40.0565	62.8919	-0.0683	0.0368	0.2623
		$k_1^2 = k_2^2 = \frac{2}{3}$	40.0611	62.8919	-0.0683	0.0368	0.2623
		$k_1^2 = k_2^2 = \frac{\pi^2}{12}$	40.0568	62.8919	-0.0683	0.0368	0.2623
		$k_1^2 = 0.8793$ $k_2^2 = 0.8793$	40.0556	62.8919	-0.0683	0.0368	0.2623
	TSDT		40.0556	62.8972	-0.0683	0.0368	0.2623
	FSDT5 [83]		40.0520	62.8900	-0.0527	0.0284	0.2622
	HSDT13 [83]		40.0520	62.8900	-0.0527	0.0284	0.2626
	RZT		40.0548	62.8961	-0.0683	0.0368	0.2623
	3D		40.0528	62.8943	-0.0683	0.0368	0.2622

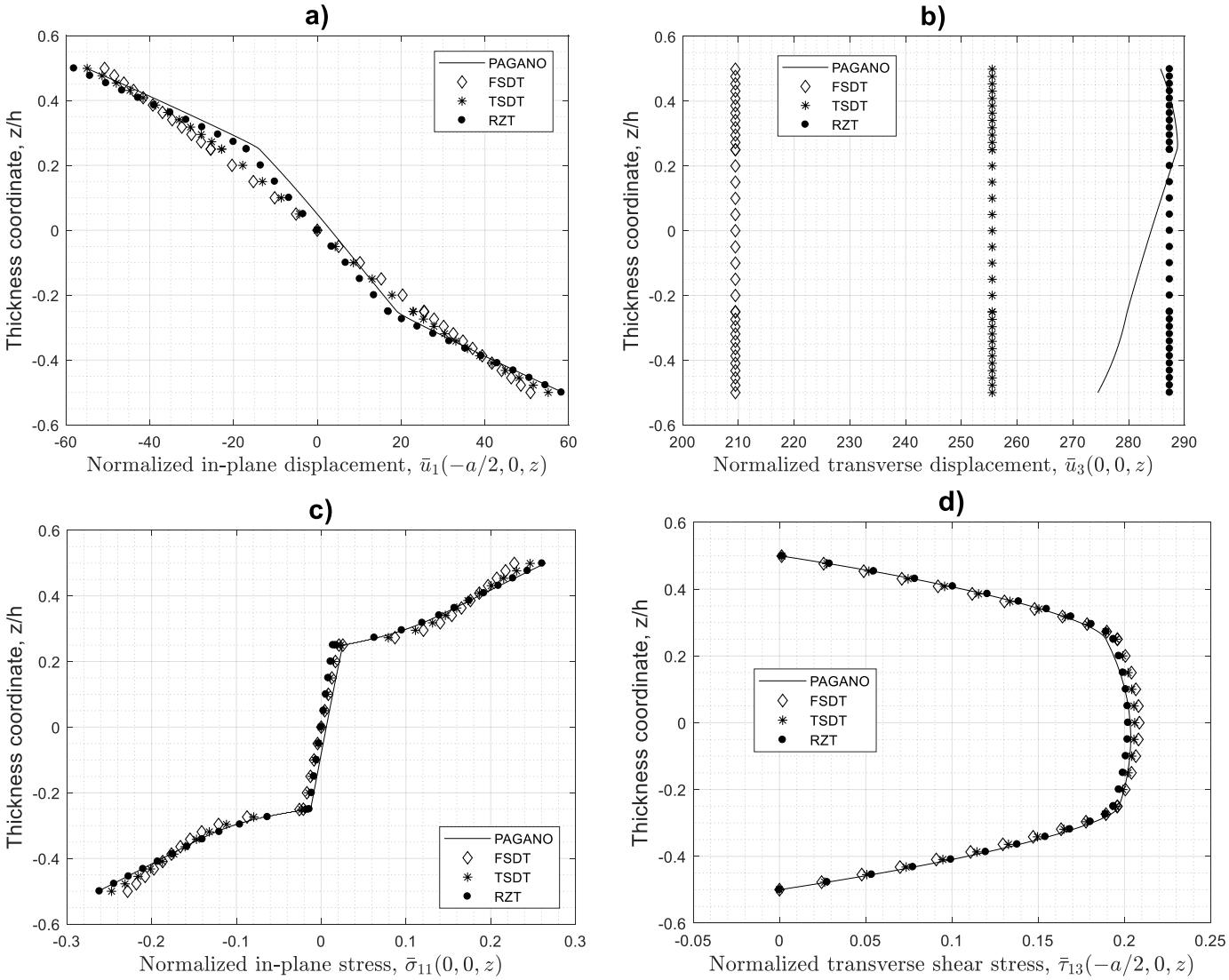

Figure 3. Non-dimensional displacement and stresses for a simply supported sandwich plate (L4) under bi-sinusoidal transverse pressure (*a*/*h*=5; *p*=10). a) non-dimensional in-plane displacement, $\bar{u}_1$; b) non-dimensional transverse displacement, $\bar{u}_3$; c) non-dimensional in-plane stress, $\bar{\sigma}_{11}$; d) non-dimensional transverse shear stress, $\bar{\tau}_{13}$. Comparison between different theories.

Figure 3 shows that there is a good agreement between the RZT solution for in-plane and transverse shear stresses and the exact solution computed using Pagano solution. The small differences are due to a compressive along transverse direction of sandwich plate not considered in RZT and other 2D theories. The superior capability of RZT, over the other 2D theories, to estimate the central deflection is shown in Figure 3-b. FSDT is not capable to reproduce the correct distribution of the in-plane displacement of sandwich plate, Figure 3-a. In particular, the core displacements are completely wrong. Reddy TSDT improves the matching for in-plane displacement but near the interface there are strong differences. Although it does not consider the effect of σ_{zz}, RZT can match very well also near the interfaces. For transverse shear stresses computed integrating the local equilibrium equation, only RZT has a good matching with 3D Pagano solution. Considering the in-plane stresses the RZT shows superior capabilities to predict the stress distribution along the thickness. Near the external surface the other theories loss their capability to predict the correct behavior.

Although for a non-sandwich FG plate the differences between the theories are not so evident (Table 6), from Figure 3 it is argued that the RZT is the better theory, with his formulation without using a shear correction factor and only linear zigzag functions, than the most used Reddy TSDT to describe the global and local behavior of FGM plate in general.

Table 8. Comparison of global and local non-dimensional quantities for a simply supported sandwich square plate (L4) with FG face-sheet under bi-sinusoidal load.

a/h	Theory		$\bar{u}_3(0,0)$	$\bar{u}_1\left(-\frac{a}{2},0,-\frac{h}{2}\right)$	$\bar{\sigma}_{11}\left(0,0,-\frac{h}{2}\right)$	$\bar{\tau}_{13}\left(-\frac{a}{2},0,0\right)$
5	FSDT	$k_1^2 = k_2^2 = 1$	0.0276	-0.0067	2.2830	0.2086
	TSDT		0.0336	-0.0073	2.4730	0.2059
	Nguyen et al [76]		0.0358	NA	2.5492	0.1870
	RZT		0.0378	-0.0077	2.6150	0.2021
	3D		0.0374	-0.0073	2.6510	0.2033

To assess RZT with orthotropic material, a simply supported rectangular $(b = 2a)$ sandwich plate (L5) with S-FGM face-sheet under bi-sinusoidal transverse pressure is considered. The solution for non-dimensional displacement and stresses of FSDT (using ad hoc shear correction factor, Raman et al [125]), Reddy TSDT and RZT are compared with the 3D Pagano approach. The grading law is the S-FGM (see, Table 1) where the external properties are ten times the internal properties, except the value of Poisson's ratio is assumed constant, the value for the exponent p is assumed to be 0.5. In Figure 4 are shown the distribution of non-dimensional displacement and stresses given by (41) are computed using the E_2 of core material.

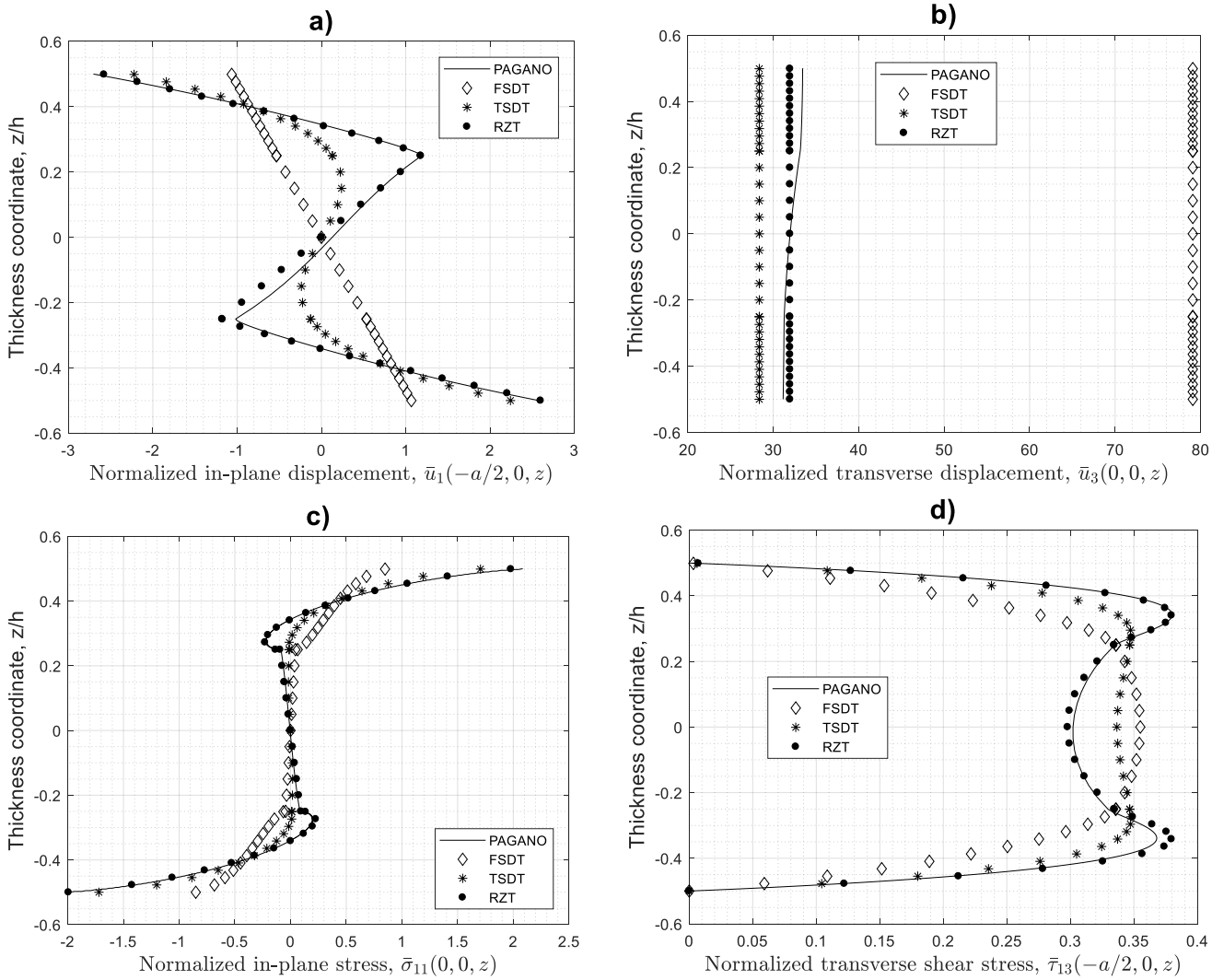

Figure 4. Non-dimensional displacement and stresses for a rectangular SSSS (b=2a) sandwich orthotropic plate (L5) with S-FGM ($p = 0.5$) face-sheet and soft core under bi-sinusoidal transverse pressure. The shear correction factor for FSDT are $k_1^2 = 0.143677$ and $k_2^2 = 0.897983$.

The plotted results clearly show the superior capability of RZT over the other 2D theories to predict the global and local behavior through the thickness for displacement and stresses if compared with the 3D Pagano solution [123].

The same previous L5 rectangular ($b = 2a$) plate with S-FG face-sheet is now considered fully clamped under constant uniform pressure. In Figure 5 are compared the results using the FSDT with Raman's shear correction factor, the Reddy TSDT and the present RZT with those obtained using MSC/MD-NASTRAN using 3D FEM solution. The model is discretized using the HEXA8 linear element. The core is built up with 16000 solid elements and for each sub-layer of face-sheet (each face-sheet is divided into 20 sublayers) has 3200 elements. Each node of the four edges are constrained with the clamped condition. The total number of nodes is 152766. The FEM model in this case is stiffer than the 2D theories.

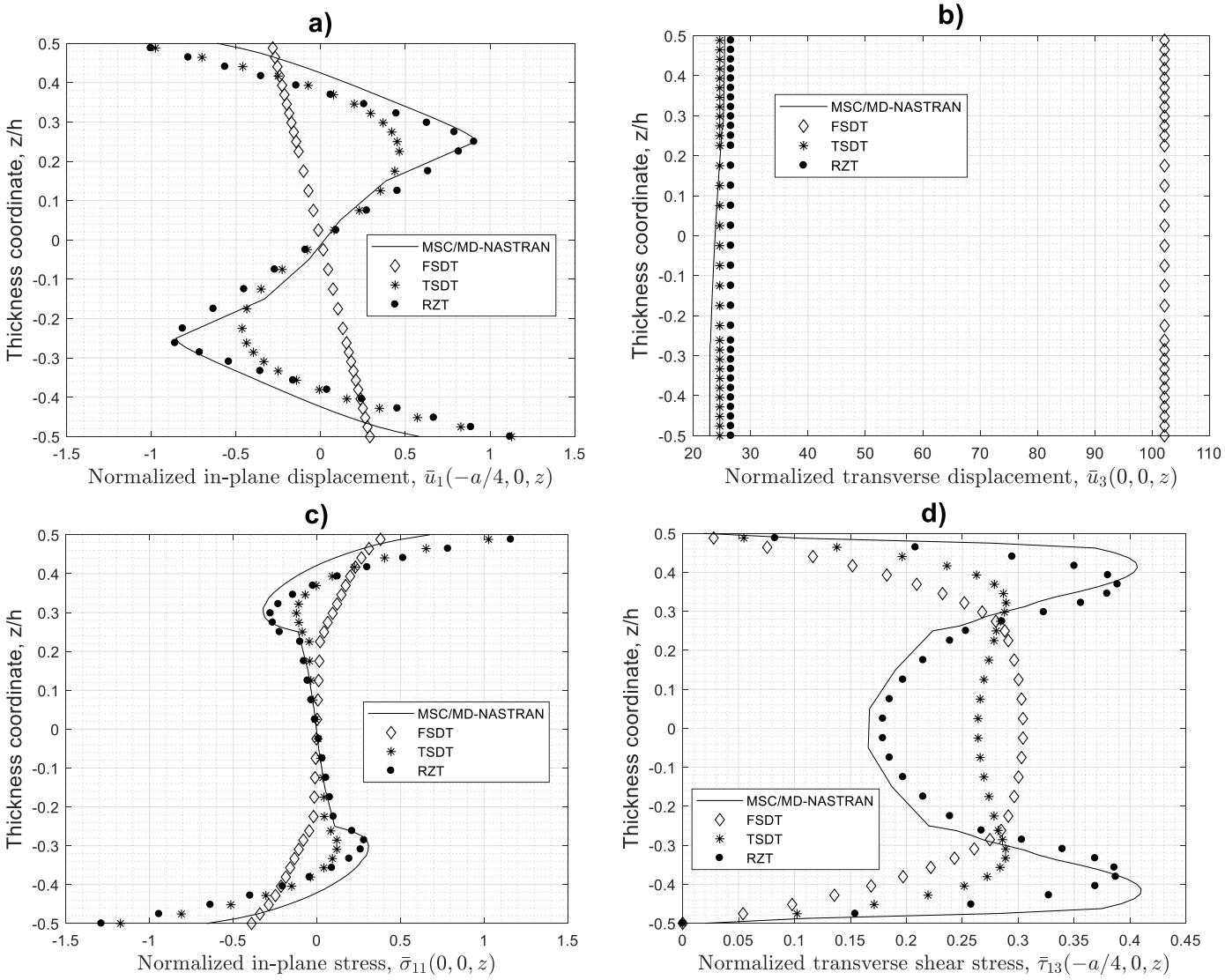

Figure 5. Non-dimensional displacement and stresses for a rectangular CCCC (b=2a) sandwich orthotropic plate (L5) with S-FGM ($p = 0.5$) under bi-sinusoidal transverse pressure. The shear correction factor [125] for FSDT are $k_1^2 = 0.1438$ and $k_2^2 = 0.8986$.

From Figure 5, although there isn't a perfect matching with the plots of 3D FEM, among the theories considered only the RZT can predict the displacement and the stresses with a good accuracy near the interfaces.

Now let us investigate the effect of grading law on the response. To do this, we consider a fully clamped rectangular ($b = 3a$) sandwich plate (L4) with different type of ceramic/metal FGM face-sheet under uniform load. The types of FGM analyzed are P-FGM, E-FGM and S-FGM (see, Table 1) with three values of exponent $p = 0.5, 1.0, 1.5$. The core-to-face-sheet thickness ratio is $h_c/h_f = 2$ and the span to thickness ratio is $a/h = 5$ (thick sandwich plate).

Table 9. Comparison of non-dimensional central deflection $\bar{u}_3 = \frac{u_3 E_2 h^2}{q_0 a^3}$ (E_2 is the young modulus of Ceramic phase) for a rectangular $(b = 3a)$ fully clamped (CCCC) sandwich plate (L4) with different FGM for face-sheets. 10 orthogonal polynomials for x_1 and x_2 directions.

Theory		P-FGM			E-FGM			S-FGM		
		$p = 0.5$	$p = 1.0$	$p = 1.5$	$p = 0.5$	$p = 1.0$	$p = 1.5$	$p = 0.5$	$p = 1.0$	$p = 1.5$
CPT		2.9488	2.3180	2.0672	3.7696	2.7512	2.3484	2.4016	2.3180	2.2724
FSDT	$k_1^2 = k_2^2 = 1$	5.0084	4.0128	3.6100	6.2244	47.2948	4.0964	4.1040	4.0128	3.9672
	$k_1^2 = k_2^2 = 5/6$	5.4188	4.3548	3.9140	6.7184	5.1224	4.4384	4.4384	4.3548	4.3092
	$k_1^2 = k_2^2 = hoc*$	6.4372	5.6544	5.3580	7.4328	6.2092	5.7228	5.7228	5.6544	5.6468
TSDT		6.1864	5.2744	4.8640	7.2428	5.9584	5.3808	5.2668	5.2744	5.2896
RZT		6.2472	5.4112	5.0768	7.2732	6.0116	54.8872	5.4568	5.4112	5.4112

*Shear correction factors [125]: P-FGM $k_1^2 = k_2^2 = 0.5895$ for $p = 0.5$; $k_1^2 = k_2^2 = 0.5071$ for $p = 1.0$; $k_1^2 = k_2^2 = 0.4664$ for $p = 1.5$. E-FGM $k_1^2 = k_2^2 = 0.6701$ for $p = 0.5$; $k_1^2 = k_2^2 = 0.5711$ for $p = 1.0$; $k_1^2 = k_2^2 = 0.5162$ for $p = 1.5$; S-FGM $k_1^2 = k_2^2 = 0.5107$ for $p = 0.5$; $k_1^2 = k_2^2 = 0.5071$ for $p = 1.0$; $k_1^2 = k_2^2 = 0.5017$ fo $p = 1.5$.

In Table 9 the effect of law of variation of properties along the thickness and the exponent p used in the grading law for the central deflection using different theories is shown.

Increasing the value of exponent p means, for this sandwich type, an increase of ceramic phase near the core interfaces. Low values of p produce face-sheets with ceramic phase only in a limited area near the external surfaces. This material effect is expressed by a variation of the flexural stiffness. Increasing the value for p decreases the stiffness of the sandwich plate.

As previously noted (Table 1), for $p = 1$, P-FGM and S-FGM give rise to the same law of distribution; so, they give the same results.

Results in Table 9 confirms what is well known. CPT under-estimates the central deflection; accuracy of FSDT is strongly related to the use of ad hoc shear correction factors, such as Raman's shear correction factor [125]. TSDT and RZT give comparable numerical results, with RZT being less computationally expensive, especially when FEM formulation is taken into account, [112–122].

3.3 Free vibration

In this section the free vibration of square and rectangular P-FGM and S-FGM plates is considered.

In the following tables, the subscript *"c"* and *"m"* indicate, respectively, the ceramic and metal mechanical properties of the plate considered.

Table 10 compares results for the first three non-dimensional circular frequencies of simply-supported (SSSS) square plates (L2) with span-to-thickness ratio $a/h = 5$, obtained using different plate theories (CPT, FSDT with different shear correction factors, TSDT, RZT) with those obtained by Zhang et al [126] with the 3D-FEM solution. Results for different values of index p are shown.

Table 10 shows a good matching of the RZT results with the 3D FEM results. The CPT over-estimates the value of frequencies. The FSDT without considering the shear correction factor increase the transverse deformability but is still too stiff if compared with the 3D FEM solution. Using an appropriate shear correction factor, the frequencies are under-estimated. With TSDT does not require a shear correction factor but the RZT results match very well with the 3D FEM for all cases without introducing any shear correction factor or using third order functions to describe the kinematics.

To assess the RZT with other boundary conditions, a rectangular $(b = 2a)$ P-FGM plate (L6) is considered. The boundary conditions considered are: SSSS, SCSC, SCSF, SSSC and SSSF. Two values of exponent p are considered. Table 11 shows results for the fundamental frequency obtained using CPT, FSDT ad hoc shear correction factor [125], TSDT and the present RZT are compared with the 3D FEM solution computed by Zhang et al [126].

Table 11 shows the non-dimensional frequencies computed using different theories and, for comparison, those obtained by Zhang et al [126] using 3D FEM approach. As can be seen, CPT over-estimates the frequencies for all type of BCs, except for SCSC case. Using FSDT with an appropriate shear correction factor the frequencies decrease. Better results, when compared with 3D FEM results, are obtained using TSDT and RZT; furthermore, RZT generally provides better results than TSDT. It should be noted that all theories give the same numerical results for SCSF and SSSF. This is explained by analysing the corresponding modal shapes: the first natural frequency is relative to a membrane mode, as can be argued by plotting the corresponding modal shape.

Table 10. Comparison of circular frequencies parameters $\left(\bar{\omega} = \frac{\omega}{h}\sqrt{\frac{\rho_c}{E_c}}\right)$ for different theories of a simply supported (SSSS) P-FGM square plate (L2) $(a/h = 5)$ with different values of p.

Mode	Theories		P-FGM			
			$p = 0.5$	$p = 1$	$p = 4$	$p = 10$
(1,1)	CPT		0.1959	0.1761	0.1522	0.1466
	FSDT	$k_1^2 = k_2^2 = 1$	0.1828	0.1650	0.1415	0.1344
		$k_1^2 = k_2^2 = \frac{5}{6}$	0.1805	0.1630	0.1396	0.1323
		$k_1^2 = k_2^2 = \frac{2}{3}$	0.1771	0.1602	0.1368	0.1292
		$k_1^2 = k_2^2 = \frac{\pi^2}{12}$	0.1803	0.1629	0.1394	0.1321
		$k_1^2 = k_2^2 = hoc$ *	0.1807	0.1630	0.1373	0.1297
	TSDT		0.1807	0.1631	0.1377	0.1294
	RZT		0.1828	0.1650	0.1397	0.1318
	3D FEM [126]		0.1818	0.1640	0.1383	0.1307
(1,2)	CPT		0.4681	0.4196	0.3601	0.3478
	FSDT	$k_1^2 = k_2^2 = 1$	0.4075	0.3687	0.3124	0.2938
		$k_1^2 = k_2^2 = \frac{5}{6}$	0.3977	0.3602	0.3046	0.2854
		$k_1^2 = k_2^2 = \frac{2}{3}$	0.3841	0.3485	0.2939	0.2739
		$k_1^2 = k_2^2 = \frac{\pi^2}{12}$	0.3970	0.3596	0.3041	0.2847
		$k_1^2 = k_2^2 = hoc$ *	0.39856	0.3601	0.2956	0.2757
	TSDT		0.3988	0.3605	0.2977	0.2768
	RZT		0.4074	0.3686	0.3057	0.2840
	3D FEM [126]		0.4033	0.3647	0.3002	0.2796
(2,2)	CPT		0.7183	0.6421	0.5473	0.5301
	FSDT	$k_1^2 = k_2^2 = 1$	0.5966	0.5404	04548	0.4249
		$k_1^2 = k_2^2 = \frac{5}{6}$	0.5778	0.5243	0.4402	0.4093
		$k_1^2 = k_2^2 = \frac{2}{3}$	0.5523	0.5023	0.4204	0.3886
		$k_1^2 = k_2^2 = \frac{\pi^2}{12}$	0.5764	0.5231	0.4391	0.4081
		$k_1^2 = k_2^2 = hoc$ *	0.5794	0.5240	0.4236	0.3919
	TSDT		0.5802	0.5252	0.4281	0.3945
	RZT		0.5962	0.5404	0.4430	0.4073
	3D FEM [126]		0.5885	0.5333	0.4329	0.3994

*Shear correction factor [125]: $k_1^2 = k_2^2 = 0.8459$ for $p = 0.5$; $k_1^2 = k_2^2 = 0.8304$ for $p = 1$; $k_1^2 = k_2^2 = 0.6901$ for $p = 4$; $k_1^2 = k_2^2 = 0.6899$ for $p = 10$.

Table 11. Comparison of fundamental circular frequencies parameters $\bar{\omega} = \frac{\omega}{h}\sqrt{\frac{\rho_m}{E_m}}$ of rectangular $(b = 2a)$ (L6) Al/ZrO_2 P-FG plate $(a/h = 5)$ with different boundary conditions for different theories. Between parenthesis the number of orthogonal polynomials used in the Ritz method.

	SSSS $(N_1 = N_2 = 8)$		SCSC $\binom{N_1 = 8}{N_2 = 10}$		SCSF $\binom{N_1 = 8}{N_2 = 10}$		SSSC $\binom{N_1 = 8}{N_2 = 10}$		SSSF $(N_1 = N_2 = 8)$	
Theory	$p = 1$	$p = 5$	$p = 1$	$p = 5$	$p = 1$	$p = 5$	$p = 1$	$p = 5$	$p = 1$	$p = 5$
CPT	0.1567	0.1599	0.1570	0.1602	0.1085	0.1024	0.1569	0.1600	0.1085	0.1024
FSDT $(k_1^2 = k_2^2 = 1)$	0.1494	0.1513	0.1621	0.1637	0.1085	0.1024	0.1550	0.1568	0.1085	0.1024
FSDT $(k_1^2 = k_2^2 = hoc)$*	0.1480	0.1487	0.1600	0.1600	0.1085	0.1024	0.1534	0.1538	0.1085	0.1024
TSDT	0.1480	0.1488	0.1571	0.1565	0.1085	0.1024	0.1522	0.1524	0.1085	0.1024
RZT	0.1493	0.1502	0.1620	0.1622	0.1085	0.1024	0.1550	0.1556	0.1085	0.1024
3D-FEM [52, 126]	0.1484	0.1493	0.1609	0.1611	0.1085	0.1024	0.1540	0.1545	0.1085	0.1024

* Shear correction factor [125]: $k_1^2 = k_2^2 = 0.8310$ for $p = 1$; $k_1^2 = k_2^2 = 0.7558$ for $p = 5$.

All theories capture the effect of changing the exponent p for P-FGM: increasing the value of the exponent, the region of metal rich increases, the global density of the plate decreases and the frequencies for the case with $p = 5$ are higher than those with $p = 1$.

For a simply supported (SSSS) square sandwich plate (L3) with S-FGM (Al/Al_2O_3) face-sheets and hard ceramic core, Table 12 collects results of the non-dimensional fundamental frequencies for different span-to-thickness ratio and exponent p for sigmoidal law (S-FGM). Results computed using CPT, FSDT with different values of shear correction factors, TSDT and RZT are compared with results computed by Singh et al [43] using a kinematic based on non-polynomial higher-order shear deformation plate theory (HOSDT) with inverse hyperbolic shape function. The comparison confirms the high accuracy of RZT.

Table 13 shows results for the fundamental frequencies of a fully clamped (CCCC) sandwich square plate (L7) with P-FGM (Al/Al_2O_3) face-sheet and metal (Al) soft core, for different values of power index p and face-to-core thickness ratios. Results computed using FSDT with two values of shear correction factors, TSDT and RZT are compared with results of 3D Ritz solution of Li et al [50]. The comparison shows a very good matching between RZT and 3D results, also for low values of h_c/h_f ratio.

Table 12. Comparison of non-dimensional fundamental circular frequencies $\bar{\omega} = \frac{\omega a^2}{h}\sqrt{\frac{\rho_m}{E_m}}$ for a (SSSS) sandwich plate (L3) with S-FGM face-sheets and hard ceramic (Al_2O_3) core.

$h_c/h_f = 2$	$p = 1$			$p = 4$			$p = 10$		
a/h	5	10	100	5	10	100	5	10	100
CPT	8.9145	9.1102	9.1776	8.6736	8.8617	8.9264	8.6263	8.8128	8.8771
FSDT $(k_1^2 = k_1^2 = 1)$	8.4240	8.9657	9.1761	8.2197	8.7285	8.9250	8.1794	8.6818	8.8757
FSDT $(k_1^2 = k_1^2 = hoc)$*	8.3750	8.9504	9.1759	8.1624	8.7106	8.9248	8.1187	8.6630	8.8755
TSDT	8.3754	8.9508	9.1760	8.1671	8.7126	8.9249	8.1261	8.6657	8.8755
RZT	8.3936	8.9564	9.1760	8.2037	8.7238	8.9250	8.1685	8.6787	8.8757
HOSDT [36]	8.3753	8.9507	9.1759	8.1677	8.7126	8.9248	8.1261	8.6657	8.8755

*Shear correction factor [125]: $k_1^2 = k_2^2 = 0.9016$ for $p = 1$; $k_1^2 = k_2^2 = 0.8791$ for $p = 4$; $k_1^2 = k_2^2 = 0.8714$ for $p = 10$.

Table 13. Comparison of non-dimensional frequencies $\bar{\omega} = \frac{\omega a^2}{h}\sqrt{\frac{\rho_m}{E_m}}$ for fully clamped (CCCC) thick (*a/h*=5) square sandwich (L7) with P-FG (Al/Al_2O_3) face-sheet and metal (Al) soft core. 10 orthogonal polynomials for x_1 and x_2 directions.

a/h=5	$p = 0.5$			$p = 1$			$p = 5$		
$\left(\frac{h_f}{h_f} - \frac{h_c}{h_f} - \frac{h_f}{h_f}\right)$	1-1-1	1-2-1	1-8-1	1-1-1	1-2-1	1-8-1	1-1-1	1-2-1	1-8-1
FSDT $(k_1^2 = k_2^2 = 1)$	14.9766	11.9595	10.2617	16.4689	13.1383	11.0083	17.2047	13.7252	11.4078
FSDT $(k_1^2 = k_2^2 = hoc)$*	12.2361	10.4082	9.48371	12.6612	10.8769	9.90075	12.8059	11.0474	10.0893
TSDT	19.4884	10.7027	9.68056	21.0519	11.3707	10.1463	21.5762	11.714	10.3644
RZT	12.7870	10.5894	9.58501	13.4844	11.1526	10.0071	13.7985	11.3839	10.2027
3D Ritz solution [50]	11.15126	10.68654	9.642492	11.83599	11.2635	10.08594	12.84633	11.91534	10.68051

*Shear correction factor [125]: for $p = 0.5$ (1-1-1) $k_1^2 = k_2^2 = 0.5630$, (1-2-1) $k_1^2 = k_2^2 = 0.5895$, (1-8-1) $k_1^2 = k_2^2 = 0.7192$; for $p = 1$ (1-1-1) $k_1^2 = k_2^2 = 0.4837$, (1-2-1) $k_1^2 = k_2^2 = 0.5071$, (1-8-1) $k_1^2 = k_2^2 = 0.6595$; $p = 1.5$ (1-1-1) $k_1^2 = k_2^2 = 0.4458$, (1-2-1) $k_1^2 = k_2^2 = 0.4664$, (1-8-1) $k_1^2 = k_2^2 = 0.6263$.

Table 14. Comparison of non-dimensional frequencies $\bar{\omega} = \frac{\omega a^2}{h}\sqrt{\frac{\rho_{core}}{E_{2_{core}}}}$ for a CCCC rectangular $(b = 2a)$ sandwich plate (L5) $(h_c/h_f = 2)$ with orthotropic S-FGM.

	Mode					
Theory	(1,1)	(1,2)	(1,3)	(1,4)	(2,1)	(2,2)
TSDT	9.0841	9.6909	10.8412	12.4611	19.2055	19.5508
RZT	8.7279	9.2844	10.3369	11.8292	18.1328	18.4569
3D FEM	9.1327	9.6420	10.6304	12.0501	18.6548	18.9359

In closing this assessment, the free vibration of a thick (span-to-thickness ratio, *a/h*=5) fully clamped (CCCC) rectangular $(b = 2a)$ sandwich S-FGM (exponent $p = 0.5$) (L5) with orthotropic material (Table 2, material O) is investigated., using TSDT, RZT and NASTRAN/PATRAN 3D FEM model used for the static analysis. The first 6 non-dimensional frequencies are computed and compared in Table 14.

Also for the free vibration case the sandwich plate (L5) has a stiffer behavior.

4. Conclusions

In this paper an assessment of the Refined Zigzag Theory (RZT) for bending and free vibration problem of functionally graded rectangular plates has been presented.

After exposing the functionally graded law for monolayer and sandwich plates the equations of motion have been derived using the D'Alembert Principle.

The Ritz method has been used here to solve the bending and the free vibration problem of simply supported and fully clamped square and rectangular plate.

Numerical analyses have been performed in order to assess the reliability of RZT to compute the maximum deflection, natural frequencies and local responses. The influence of FGM law type, type of load, span-to-thickness ratio, aspect ratio, core-to-face thickness ratio, materials has been taken in consideration. Other theories such as CPT, First Order Shear Deformation Theory (FSDT) with different shear correction factor, Reddy TSDT, 3D exact solution of Pagano, 3D FEM solution and other results obtained by current literature have been considered for comparison purpose. Firstly, the numerical studies showed the accuracy of approximate Ritz method to compute the maximum deflection, local stresses and frequencies for an E-FGM orthotropic sandwich plate. Several numerical studies for bending problem have been performed and the superior accuracy of RZT to predict the global response (maximum deflection and frequencies) and local quantities (distribution of in-plane displacement, in-plane and transverse shear stresses through the thickness) of FGM sandwich plates has been shown. The RZT although uses only linear function without any shear correction factor gives more accurate results if compared with the exact solution and 3D FEM results. Using an appropriate shear correction factor for FSDT based on energy consideration [125] over-estimates the deflection and under-estimates the frequencies. The Reddy TSDT, typically used in literature to describe the behavior of FGM structures, is not capable like the RZT to catch the distribution of local response for an orthotropic FGM sandwich plate.

It is concluded that the RZT generally predicts the global (deflection and frequencies) and local (displacement and stress distributions) response of FGM sandwich plates, more accurately than first-order (FSDT) and third-order (TSDT) shear deformation theories, while retaining its simplicity.

In concluding this assessment, from a computational cost point of view, it is of interest to note that FEM formulations based on RZT require only C^0 shape functions, like FSDT based finite elements.

Appendix A

The Ritz method-Assumed trial functions

As we said, in the Ritz method the *trial* functions (also known as generalized functions) must be linearly independent and individually satisfy at least the kinematic boundary conditions, i.e., they must be admissible functions. The choice of the admissible functions is a very important step because the convergence rate of the approximate solution depends on them. Commonly used admissible functions are polynomials, although there are examples where other types of admissible functions have been used; for example, characteristic (modal shapes) functions of problem of low order, i.e., modes of beam for the analysis of vibration of plates and so on.

In this research, the Gram-Schmidt polynomials are used as generalized Ritz functions. The Gram-Schmidt polynomials can accommodate various kinematic boundary conditions. Compared to other polynomial admissible functions they present fast convergence characteristics in our experience. Moreover, being orthogonal, they yield a diagonal mass matrix Here below a brief description of the procedure for constructing such polynomials is initially established for one-dimensional problem, whereas for two-dimensional applications simple product of one-dimensional polynomial are used, using the variable separation technique.

Let $g\left(\xi\right)$ be the one-dimensional Gram-Schmidt polynomial with $\xi \in [-1,1]$; the recurrence formula is

$$g_{m+1}(\xi) \equiv \left(\xi - A_m\right) g_m(\xi) - B_m g_{m-1}(\xi) \qquad \text{(m=1,2,…)} \tag{A.1}$$

with

$$A_m \equiv \frac{\int_{-1}^{+1} \xi g_{m+1}^2(\xi)\, d\xi}{\int_{-1}^{+1} g_m^2(\xi)\, d\xi}, \quad B_m \equiv \frac{\int_{-1}^{+1} g_m^2(\xi)\, d\xi}{\int_{-1}^{+1} g_{m-1}^2(\xi)\, d\xi} \tag{A.2}$$

and

$$g_0(\xi) = 0; \qquad g_1(\xi) = b_1\left(\xi\right)^{\Omega_1} b_2\left(\xi\right)^{\Omega_2} \tag{A.3}$$

where in general

$$b_i\left(\xi\right) = 0 \tag{A.4}$$

is the equation of the edge *i*th. For the one-dimensional problem at the hand,

$$b_1\left(\xi\right) = 1 + \xi \quad \text{and} \quad b_2\left(\xi\right) = 1 - \xi. \tag{A.5}$$

In Eq. (A.3) the values of the exponents depend on the boundary conditions: 0 if the function does not vanish, 1 if the function vanishes (for the problem at hand, see Table A.2).

As we said, the two dimensional admissible functions are written as product of one-dimensional Gram-Schmidt polynomials. Thus for the general unknown function (33), we write

$$\hat{f}\left(\xi_1,\xi_2,t\right)=\sum_{p=1}^{P(f)}\sum_{r=1}^{R(f)}C_{pr}^{(f)}(t)g_p^{(f)}\left(\xi_1\right)g_r^{(f)}\left(\xi_2\right)=\sum_{m=1}^{M(f)}C_m^{(f)}(t)g_m^{(f)}\left(\xi_1,\xi_2\right) \tag{A.6}$$

with

$$m=\left(p-1\right)R\left(f\right)+r \tag{A.7}$$

The first basis function is given by

$$g_1^{(f)}\left(\xi_1,\xi_2\right)=\prod_{j=1}^{n_l}\left[\chi_j\left(\xi_1,\xi_2\right)\right]^{\Omega_j^{(f)}} \tag{A.8}$$

where n_l gives the number of the plate edges (for quadrilateral plate, $n_l=4$), $\chi_j(\xi_1,\xi_2)=0$ is the equations of the *j*th edge of the plate, the exponents Ω_j are chosen such that the geometric (prescribed) boundary condition on the edge for the function $\hat{f}\left(\xi_1,\xi_2,t\right)$ be satisfied.

For example, for the square plate shown in Fig. 1, the functions $\chi_j(\xi_1,\xi_2)$ are:

$$\chi_1\left(\xi_1,\xi_2\right)=\left(\xi_1+1\right),\ \chi_2\left(\xi_1,\xi_2\right)=\left(\xi_2+1\right),\ \chi_3\left(\xi_1,\xi_2\right)=\left(\xi_1-1\right),\ \chi_4\left(\xi_1,\xi_2\right)=\left(\xi_2-1\right)$$

The prescribed (geometric) boundary condition are given in Table A.1 (see, Tessler et al [107, 108]).

Table A.1. Prescribed (geometric) boundary conditions of RZT.

Edge F	u_α, w, θ_α, ψ_α free
Edge $\xi_1=\mp1$ SS	$u_1=w=\theta_1=\psi_1=0$; u_2, θ_2, ψ_2 free
Edge $\xi_2=\mp1$ SS	$u_2=w=\theta_2=\psi_2=0$; u_1, θ_1, ψ_1 free
Edge C	$u_\alpha=w=\theta_\alpha=\psi_\alpha=0$
F=free, C= clamped, SS=simply supported	

The exponents $\Omega_j^{(f)}$ for the classical geometric boundary condition of RZT are given in Table A.2.

Table A.2. Exponents for the classical geometric boundary conditions.

edge $\xi_1 = \mp 1$ SS	$\Omega_j^{u_1} = \Omega_j^{\theta_1} = \Omega_j^{\psi_1} = 0$ $\Omega_j^{u_2} = \Omega_j^{\theta_2} = \Omega_j^{\psi_2} = 1$
edge $\xi_2 = \mp 1$ SS	$\Omega_j^{u_1} = \Omega_j^{\theta_1} = \Omega_j^{\psi_1} = 1$ $\Omega_j^{u_2} = \Omega_j^{\theta_2} = \Omega_j^{\psi_2} = 0$
edge SS	$\Omega_j^{w} = 1$
edge F	$\Omega_j^{f} = 0$
edge C	$\Omega_j^{f} = 1$

References

[1] Reddy JN, Miravete A. *Practical Analysis of Composite Laminates*. CRC Press, Inc. Epub ahead of print 1995. DOI: 10.1201/9780203742594.

[2] Koizumi M, Niino M. Overview of FGM Research in Japan. *MRS Bulletin* 1995; 20: 19–21.

[3] Koizumi M. FGM activities in Japan. *Composites Part B: Engineering* 1997; 28: 1–4.

[4] Bohidar SK, Sharma R, Mishra PR. Functionally Graded Materials: A Critical Review. 2014; 1: 13.

[5] Udupa G, Rao SS, Gangadharan KV. Functionally Graded Composite Materials: An Overview. *Procedia Materials Science* 2014; 5: 1291–1299.

[6] Swaminathan K, Sangeetha DM. Thermal analysis of FGM plates – A critical review of various modeling techniques and solution methods. *Composite Structures* 2017; 160: 43–60.

[7] Mahamood RM, Akinlabi ET. Types of Functionally Graded Materials and Their Areas of Application. In: Mahamood RM, Akinlabi ET (eds) *Functionally Graded Materials*. Cham: Springer International Publishing, pp. 9–21.

[8] Birman V, Byrd LW. Modeling and Analysis of Functionally Graded Materials and Structures. *Appl Mech Rev* 2007; 60: 195–216.

[9] Zuiker JR. Functionally graded materials: Choice of micromechanics model and limitations in property variation. *Composites Engineering* 1995; 5: 807–819.

[10] Yin HM, Sun LZ, Paulino GH. Micromechanics-based elastic model for functionally graded materials with particle interactions. *Acta Materialia* 2004; 52: 3535–3543.

[11] Klusemann B, Böhm HJ, Svendsen B. Homogenization methods for multi-phase elastic composites with non-elliptical reinforcements: Comparisons and benchmarks. *European Journal of Mechanics - A/Solids* 2012; 34: 21–37.

[12] Loja MAR, Barbosa JI, Mota Soares CM. A study on the modeling of sandwich functionally graded particulate composites. *Composite Structures* 2012; 94: 2209–2217.

[13] Shen H-S, Wang Z-X. Assessment of Voigt and Mori–Tanaka models for vibration analysis of functionally graded plates. *Composite Structures* 2012; 94: 2197–2208.

[14] Gupta A, Talha M. Recent development in modeling and analysis of functionally graded materials and structures. *Progress in Aerospace Sciences* 2015; 79: 1–14.

[15] Ashwinkumar AK. Review on functionally graded materials and various theories. *International Research Journal of Engineering and Technology* 2017; 04: 890–893.

[16] Srividhya S, Basant K, Gupta RK, et al. Influence of the homogenization scheme on the bending response of functionally graded plates. *Acta Mech* 2018; 229: 4071–4089.

[17] Bilouei BS, Kolahchi R, Bidgoli MR. Buckling of concrete columns retrofitted with Nano-Fiber Reinforced Polymer (NFRP). *Computers and Concrete* 2016; 18: 1053–1063.

[18] Zamanian M, Kolahchi R, Bidgoli MR. Agglomeration effects on the buckling behaviour of embedded concrete columns reinforced with SiO_2 nano-particles. *Wind and Structures* 2017; 24: 43–57.

[19] Amnieh HB, Zamzam MS, Kolahchi R. Dynamic analysis of non-homogeneous concrete blocks mixed by SiO_2 nanoparticles subjected to blast load experimentally and theoretically. *Construction and Building Materials* 2018; 174: 633–644.

[20] Hosseini H, Kolahchi R. Seismic response of functionally graded-carbon nanotubes-reinforced submerged viscoelastic cylindrical shell in hygrothermal environment. *Physica E: Low-dimensional Systems and Nanostructures* 2018; 102: 101–109.

[21] Fakhar A, Kolahchi R. Dynamic buckling of magnetorheological fluid integrated by visco-piezo-GPL reinforced plates. *International Journal of Mechanical Sciences* 2018; 144: 788–799.

[22] Hajmohammad MH, Kolahchi R, Zarei MS, et al. Earthquake induced dynamic deflection of submerged viscoelastic cylindrical shell reinforced by agglomerated CNTs considering thermal and moisture effects. *Composite Structures* 2018; 187: 498–508.

[23] Hajmohammad MH, Maleki M, Kolahchi R. Seismic response of underwater concrete pipes conveying fluid covered with nano-fiber reinforced polymer layer. *Soil Dynamics and Earthquake Engineering* 2018; 110: 18–27.

[24] Golabchi H, Kolahchi R, Bidgoli MR. Vibration and instability analysis of pipes reinforced by SiO_2 nanoparticles considering agglomeration effects. *Computers and Concrete* 2018; 21: 431–440.

[25] Zarei MS, Kolahchi R, Hajmohammad MH, et al. Seismic response of underwater fluid-conveying concrete pipes reinforced with SiO2 nanoparticles and fiber reinforced polymer (FRP) layer. *Soil Dynamics and Earthquake Engineering* 2017; 103: 76–85.

[26] Hajmohammad MH, Farrokhian A, Kolahchi R. Smart control and vibration of viscoelastic actuator-multiphase nanocomposite conical shells-sensor considering hygrothermal load based on layerwise theory. *Aerospace Science and Technology* 2018; 78: 260–270.

[27] Arani AJ, Kolahchi R. Buckling analysis of embedded concrete columns armed with carbon nanotubes. *Computers and Concrete* 2016; 17: 567–578.

[28] Hajmohammad MH, Zarei MS, Nouri A, et al. Dynamic buckling of sensor/functionally graded-carbon nanotube-reinforced laminated plates/actuator based on sinusoidal-visco-piezoelasticity theories. *Jnl of Sandwich Structures & Materials* 2017; 1099636217720373.

[29] Kolahchi R, Zarei MS, Hajmohammad MH, et al. Wave propagation of embedded viscoelastic FG-CNT-reinforced sandwich plates integrated with sensor and actuator based on refined zigzag theory. *International Journal of Mechanical Sciences* 2017; 130: 534–545.

[30] Madani H, Hosseini H, Shokravi M. Differential cubature method for vibration analysis of embedded FG-CNT-reinforced piezoelectric cylindrical shells subjected to uniform and non-uniform temperature distributions. *Steel and Composite Structures* 2016; 22: 889–913.

[31] Kolahchi R, Safari M, Esmailpour M. Dynamic stability analysis of temperature-dependent functionally graded CNT-reinforced visco-plates resting on orthotropic elastomeric medium. *Composite Structures* 2016; 150: 255–265.

[32] Shakeri M, Mirzaeifar R. Static and Dynamic Analysis of Thick Functionally Graded Plates with Piezoelectric Layers Using Layerwise Finite Element Model. *Mechanics of Advanced Materials and Structures* 2009; 16: 561–575.

[33] Vo-Duy T, Ho-Huu V, Nguyen-Thoi T. Free vibration analysis of laminated FG-CNT reinforced composite beams using finite element method. *Front Struct Civ Eng* 2018; 13.

[34] Pandey S, Pradyumna S. Analysis of functionally graded sandwich plates using a higher-order layerwise theory. *Composites Part B: Engineering* 2018; 153: 325–336.

[35] Mohammadimehr M, Mostafavifar M. Free vibration analysis of sandwich plate with a transversely flexible core and FG-CNTs reinforced nanocomposite face sheets subjected to magnetic field and temperature-dependent material properties using SGT. *Composites Part B: Engineering* 2016; 94: 253–270.

[36] Lee W-H, Han S-C, Park W-T. A refined higher order shear and normal deformation theory for E-, P-, and S-FGM plates on Pasternak elastic foundation. *Composite Structures* 2015; 122: 330–342.

[37] Meziane MAA, Abdelaziz HH, Tounsi A. An efficient and simple refined theory for buckling and free vibration of exponentially graded sandwich plates under various boundary conditions. *Journal of Sandwich Structures & Materials* 2014; 16: 293–318.

[38] Chi S-H, Chung Y-L. Mechanical behavior of functionally graded material plates under transverse load—Part I: Analysis. *International Journal of Solids and Structures* 2006; 43: 3657–3674.

[39] Chi S-H, Chung Y-L. Mechanical behavior of functionally graded material plates under transverse load—Part II: Numerical results. *International Journal of Solids and Structures* 2006; 43: 3675–3691.

[40] Jha DK, Kant T, Singh RK. A critical review of recent research on functionally graded plates. *Composite Structures* 2013; 96: 833–849.

[41] Sobhy M. Buckling and free vibration of exponentially graded sandwich plates resting on elastic foundations under various boundary conditions. *Composite Structures* 2013; 99: 76–87.

[42] Anju M, Subha K. A review on functionally graded plate. *International Research Journal of Engineering and Technology* 2018; 05: 75–81.

[43] Singh SJ, Harsha SP. Exact Solution for Free Vibration and Buckling of Sandwich S-FGM Plates on Pasternak Elastic Foundation with Various Boundary Conditions. *International Journal of Structural Stability and Dynamics* 2018; 1950028.

[44] Birman V, Kardomateas GA. Review of current trends in research and applications of sandwich structures. *Composites Part B: Engineering* 2018; 142: 221–240.

[45] Thai H-T, Kim S-E. A review of theories for the modeling and analysis of functionally graded plates and shells. *Composite Structures* 2015; 128: 70–86.

[46] Sayyad AS, Ghugal YM. Modeling and analysis of functionally graded sandwich beams: A review. *Mechanics of Advanced Materials and Structures* 2018; 1–20.

[47] Reddy JN. Analysis of functionally graded plates. *International Journal for Numerical Methods in Engineering* 2000; 47: 663–684.

[48] Pan E. Exact Solution for Functionally Graded Anisotropic Elastic Composite Laminates. *Journal of Composite Materials* 2003; 37: 1903–1920.

[49] Pan E, Han F. Exact solution for functionally graded and layered magneto-electro-elastic plates. *International Journal of Engineering Science* 2005; 43: 321–339.

[50] Li Q, Iu VP, Kou KP. Three-dimensional vibration analysis of functionally graded material sandwich plates. *Journal of Sound and Vibration* 2008; 311: 498–515.

[51] Kashtalyan M. Three-dimensional elasticity solution for bending of functionally graded rectangular plates. *European Journal of Mechanics - A/Solids* 2004; 23: 853–864.

[52] Jin G, Su Z, Shi S, et al. Three-dimensional exact solution for the free vibration of arbitrarily thick functionally graded rectangular plates with general boundary conditions. *Composite Structures* 2014; 108: 565–577.

[53] Neves AMA, Ferreira AJM, Carrera E, et al. A quasi-3D sinusoidal shear deformation theory for the static and free vibration analysis of functionally graded plates. *Composites Part B: Engineering* 2012; 43: 711–725.

[54] Neves AMA, Ferreira AJM, Carrera E, et al. A quasi-3D hyperbolic shear deformation theory for the static and free vibration analysis of functionally graded plates. *Composite Structures* 2012; 94: 1814–1825.

[55] Neves AMA, Ferreira AJM, Carrera E, et al. Static, free vibration and buckling analysis of isotropic and sandwich functionally graded plates using a quasi-3D higher-order shear deformation theory and a meshless technique. *Composites Part B: Engineering* 2013; 44: 657–674.

[56] Hebali Habib, Tounsi Abdelouahed, Houari Mohammed Sid Ahmed, et al. New Quasi-3D Hyperbolic Shear Deformation Theory for the Static and Free Vibration Analysis of Functionally Graded Plates. *Journal of Engineering Mechanics* 2014; 140: 374–383.

[57] Thai H-T, Vo TP, Bui TQ, et al. A quasi-3D hyperbolic shear deformation theory for functionally graded plates. *Acta Mech* 2014; 225: 951–964.

[58] Farzam-Rad SA, Hassani B, Karamodin A. Isogeometric analysis of functionally graded plates using a new quasi-3D shear deformation theory based on physical neutral surface. *Composites Part B: Engineering* 2017; 108: 174–189.

[59] Abrate S, Di Sciuva M. Equivalent single layer theories for composite and sandwich structures: A review. *Composite Structures* 2017; 179: 482–494.

[60] Abrate S, Di Sciuva M. Multilayer Models for Composite and Sandwich Structures. In: *Comprehensive Composite Materials II*. Elsevier, pp. 399–425.

[61] Ferreira AJM, Batra RC, Roque CMC, et al. Static analysis of functionally graded plates using third-order shear deformation theory and a meshless method. *Composite Structures* 2005; 69: 449–457.

[62] Zenkour AM. A comprehensive analysis of functionally graded sandwich plates: Part 1—Deflection and stresses. *International Journal of Solids and Structures* 2005; 42: 5224–5242.

[63] Zenkour AM. A comprehensive analysis of functionally graded sandwich plates: Part 2—Buckling and free vibration. *International Journal of Solids and Structures* 2005; 42: 5243–5258.

[64] Nguyen T-K, Sab K, Bonnet G. First-order shear deformation plate models for functionally graded materials. *Composite Structures* 2008; 83: 25–36.

[65] Bessaim A, Houari MS, Tounsi A, et al. A new higher-order shear and normal deformation theory for the static and free vibration analysis of sandwich plates with functionally graded isotropic face sheets. *Journal of Sandwich Structures & Materials* 2013; 15: 671–703.

[66] Pradhan KK, Chakraverty S. Free vibration of Euler and Timoshenko functionally graded beams by Rayleigh–Ritz method. *Composites Part B: Engineering* 2013; 51: 175–184.

[67] Taj MG, Chakrabarti A, Talha M. Bending analysis of functionally graded skew sandwich plates with through-the thickness displacement variations. *Jnl of Sandwich Structures & Materials* 2014; 16: 210–248.

[68] Tounsi A, Houari MSA, Benyoucef S, et al. A refined trigonometric shear deformation theory for thermoelastic bending of functionally graded sandwich plates. *Aerospace Science and Technology* 2013; 24: 209–220.

[69] Xiang S, Kang G, Yang M, et al. Natural frequencies of sandwich plate with functionally graded face and homogeneous core. *Composite Structures* 2013; 96: 226–231.

[70] Zenkour AM. Bending analysis of functionally graded sandwich plates using a simple four-unknown shear and normal deformations theory. *Jnl of Sandwich Structures & Materials* 2013; 15: 629–656.

[71] Nguyen V-H, Nguyen T-K, Thai H-T, et al. A new inverse trigonometric shear deformation theory for isotropic and functionally graded sandwich plates. *Composites Part B: Engineering* 2014; 66: 233–246.

[72] Redddy BS, Kumar JS, Reddy CE, et al. Free Vibration Behaviour of Functionally Graded Plates Using Higher-Order Shear Deformation Theory. *Journal of Applied Science and Engineering* 2014; 17: 231–241.

[73] Redddy BS, Kumar JS, Reddy CE, et al. Static Bending Behavior of Functionally Graded Plates Subjected to Mechanical Loading. 2014; 8: 14.

[74] Mahi A, Adda Bedia EA, Tounsi A. A new hyperbolic shear deformation theory for bending and free vibration analysis of isotropic, functionally graded, sandwich and laminated composite plates. *Applied Mathematical Modelling* 2015; 39: 2489–2508.

[75] Mantari JL, Granados EV. A refined FSDT for the static analysis of functionally graded sandwich plates. *Thin-Walled Structures* 2015; 90: 150–158.

[76] Nguyen KT, Thai TH, Vo TP. A refined higher-order shear deformation theory for bending, vibration and buckling analysis of functionally graded sandwich plates. *Steel and Composite Structures* 2015; 18: 91–120.

[77] Bennoun M, Houari MSA, Tounsi A. A novel five-variable refined plate theory for vibration analysis of functionally graded sandwich plates. *Mechanics of Advanced Materials and Structures* 2016; 23: 423–431.

[78] Tounsi A, Houari MSA, Bessaim A. A new 3-unknowns non-polynomial plate theory for buckling and vibration of functionally graded sandwich plate. *Structural Engineering and Mechanics* 2016; 60: 547–565.

[79] Singh H, Hazarika BC, Dey S. Low Velocity Impact Responses of Functionally Graded Plates. *Procedia Engineering* 2017; 173: 264–270.

[80] Kolahchi R, Keshtegar B, Fakhar MH. Optimization of dynamic buckling for sandwich nanocomposite plates with sensor and actuator layer based on sinusoidal-visco-piezoelasticity theories using Grey Wolf algorithm. *Jnl of Sandwich Structures & Materials* 2017; 1099636217731071.

[81] Kolahchi R. A comparative study on the bending, vibration and buckling of viscoelastic sandwich nano-plates based on different nonlocal theories using DC, HDQ and DQ methods. *Aerospace Science and Technology* 2017; 66: 235–248.

[82] Pandey S, Pradyumna S. Free vibration of functionally graded sandwich plates in thermal environment using a layerwise theory. *European Journal of Mechanics - A/Solids* 2015; 51: 55–66.

[83] Natarajan S, Ganapathi M. Bending and vibration of functionally graded material sandwich plates using an accurate theory. *Finite Elements in Analysis and Design* 2012; 57: 32–42.

[84] Thai H-T, Vo TP. A new sinusoidal shear deformation theory for bending, buckling, and vibration of functionally graded plates. *Applied Mathematical Modelling* 2013; 37: 3269–3281.

[85] Thai H-T, Nguyen T-K, Vo TP, et al. Analysis of functionally graded sandwich plates using a new first-order shear deformation theory. *European Journal of Mechanics - A/Solids* 2014; 45: 211–225.

[86] Iurlaro L, Gherlone M, Di Sciuva M. Bending and free vibration analysis of functionally graded sandwich plates using the Refined Zigzag Theory. *Jnl of Sandwich Structures & Materials* 2014; 16: 669–699.

[87] Elishakoff I, Gentilini C. Three-Dimensional Flexure of Rectangular Plates Made of Functionally Graded Materials. *Journal of Applied Mechanics* 2005; 72: 788.

[88] Kumar Y. Free Vibration of Two-Directional Functionally Graded Annular Plates Using Chebyshev Collocation Technique and Differential Quadrature Method. *Int J Str Stab Dyn* 2014; 15: 1450086.

[89] Das M, Barut A, Madenci E, et al. A triangular plate element for thermo-elastic analysis of sandwich panels with a functionally graded core. *International Journal for Numerical Methods in Engineering* 2006; 68: 940–966.

[90] Xiang S, Jin Y, Bi Z, et al. A n-order shear deformation theory for free vibration of functionally graded and composite sandwich plates. *Composite Structures* 2011; 93: 2826–2832.

[91] Xiang S, Kang G. Static analysis of functionally graded plates by the various shear deformation theory. *Composite Structures* 2013; 99: 224–230.

[92] Zhao X, Lee YY, Liew KM. Free vibration analysis of functionally graded plates using the element-free kp-Ritz method. *Journal of Sound and Vibration* 2009; 319: 918–939.

[93] Zuo H, Yang Z, Chen X, et al. Bending, Free Vibration and Buckling Analysis of Functionally Graded Plates via Wavelet Finite Element Method. *Computers, Materials and Continua* 2014; 44: 167–204.

[94] Gupta A, Talha M. Influence of porosity on the flexural and vibration response of gradient plate using nonpolynomial higher-order shear and normal deformation theory. *Int J Mech Mater Des* 2018; 14: 277–296.

[95] Gupta A, Talha M. Influence of Porosity on the Flexural and Free Vibration Responses of Functionally Graded Plates in Thermal Environment. *Int J Str Stab Dyn* 2017; 18: 1850013.

[96] Gupta A, Talha M. Influence of micro-structural defects on post-buckling and large-amplitude vibration of geometrically imperfect gradient plate. *Nonlinear Dyn* 2018; 94: 39–56.

[97] Kiani Y, Sadighi M, Salami SJ, et al. Low velocity impact response of thick FGM beams with general boundary conditions in thermal field. *Composite Structures* 2013; 104: 293–303.

[98] Yahia SA, Atmane HA, Houari MSA, et al. Wave propagation in functionally graded plates with porosities using various higher-order shear deformation plate theories. *Structural Engineering and Mechanics* 2015; 53: 1143–1165.

[99] Bousahla AA, Benyoucef S, Tounsi A, et al. On thermal stability of plates with functionally graded coefficient of thermal expansion. *Structural Engineering and Mechanics* 2016; 60: 313–335.

[100] Chauhan PK, Khan IA. Review on Analysis of Functionally Graded Material Beam Type Structure. *International Journal of Advanced Mechanical Engineering* 2014; 4: 299–306.

[101] Dai H-L, Rao Y-N, Dai T. A review of recent researches on FGM cylindrical structures under coupled physical interactions, 2000–2015. *Composite Structures* 2016; 152: 199–225.

[102] Kumar Y. The Rayleigh–Ritz method for linear dynamic, static and buckling behavior of beams, shells and plates: A literature review. *Journal of Vibration and Control* 2018; 24: 1205–1227.

[103] Moreno-García P, dos Santos JVA, Lopes H. A Review and Study on Ritz Method Admissible Functions with Emphasis on Buckling and Free Vibration of Isotropic and Anisotropic Beams and Plates. *Archives of Computational Methods in Engineering* 2018; 25: 785–815.

[104] Tessler A, Di Sciuva M, Gherlone M. Refinement of Timoshenko Beam Theory for Composite and Sandwich Beams using Zigzag Kinematics. *NASA/TP-2007-215086* 2007; 1–45.

[105] Tessler A, Di Sciuva M, Gherlone M. A Refined Zigzag Beam Theory for Composite and Sandwich Beams. *Journal of Composite Materials* 2009; 43: 1051–1081.

[106] Di Sciuva M, Gherlone M, Tessler A. A Robust and Consistent First-Order Zigzag Theory for Multilayered Beams. In: Gilat R, Banks-Sills L (eds) *Advances in Mathematical Modeling and Experimental Methods for Materials and Structures: The Jacob Aboudi Volume*. Dordrecht: Springer Netherlands, pp. 255–268.

[107] Tessler A, Sciuva MD, Gherlone M. Refined Zigzag Theory for Laminated Composite and Sandwich Plates. *NASA/TP-2009-215561* 2009; 52.

[108] Tessler A, Di Sciuva M, Gherlone M. A consistent refinement of first-order shear-deformation theory for laminated composite and sandwich plates using improved zigzag kinematics. 2010; 5: 341–367.

[109] Versino D. *Refined theories and Discontinuous Galerkin methods for the analysis of multilayered composite structures*. PhD Thesis, Politecnico di Torino, 2012.

[110] Iurlaro L, Gherlone M, Di Sciuva M, et al. Assessment of the Refined Zigzag Theory for bending, vibration, and buckling of sandwich plates: a comparative study of different theories. *Composite Structures* 2013; 106: 777–792.

[111] Gherlone M. On the Use of Zigzag Functions in Equivalent Single Layer Theories for Laminated Composite and Sandwich Beams: A Comparative Study and Some Observations on External Weak Layers. *J Appl Mech* 2013; 80: 061004-061004–19.

[112] Iurlaro L. *Development of refined models for multilayered composite and sandwich structures: analytical formulation, FEM implementation and experimental assessment*. PhD Thesis, Politecnico di Torino, 2015.

[113] Gherlone M, Tessler A, Di Sciuva M. C0 beam elements based on the Refined Zigzag Theory for multilayered composite and sandwich laminates. *Composite Structures* 2011; 93: 2882–2894.

[114] Versino D, Gherlone M, Mattone MC, et al. C0 triangular elements based on the Refined Zigzag Theory for multilayered composite and sandwich plates. 2013; 44B: 218–230.

[115] Versino D, Gherlone M, Di Sciuva M. Four-node shell element for doubly curved multilayered composites based on the Refined Zigzag Theory. 2014; 118: 392–402.

[116] Treviso A, Mundo D, Tournour M. A C0-continuous RZT beam element for the damped response of laminated structures. *Composite Structures* 2015; 131: 987–994.

[117] Treviso A, Mundo D, Tournour M. Dynamic response of laminated structures using a Refined Zigzag Theory shell element. *Composite Structures* 2017; 159: 197–205.

[118] Oñate E, Eijo A, Oller S. Simple and accurate two-noded beam element for composite laminated beams using a refined zigzag theory. *Computer Methods in Applied Mechanics and Engineering* 2012; 213–216: 362–382.

[119] Oñate E. *Structural Analysis with the Finite Element Method. Linear Statics: Volume 2: Beams, Plates and Shells*. Springer Netherlands, https://www.springer.com/la/book/9781402087424 (2013, accessed 14 February 2019).

[120] Di Sciuva M, Gherlone M, Iurlaro L, et al. A class of higher-order C0 composite and sandwich beam elements based on the Refined Zigzag Theory. *Composite Structures* 2015; 132: 784–803.

[121] Groh RM, Weaver PM, Tessler A. Application of the Refined Zigzag Theory to the Modeling of Delaminations in Laminated Composites. 2015; 22.

[122] Kefal A, Tessler A, Oterkus E. *An Efficient Inverse Finite Element Method for Shape and Stress Sensing of Laminated Composite and Sandwich Plates and Shells*. Report, NASA, https://strathprints.strath.ac.uk/65515/ (31 July 2018, accessed 14 February 2019).

[123] Pagano NJ. Exact Solutions for Rectangular Bidirectional Composites and Sandwich Plates. *Journal of Composite Materials* 1970; 4: 20–34.

[124] Reddy JN. A Simple Higher-Order Theory for Laminated Composite Plates. *J Appl Mech* 1984; 51: 745–752.

[125] Madabhusi-Raman P, Davalos JF. Static shear correction factor for laminated rectangular beams. *Composites Part B: Engineering* 1996; 27: 285–293.

[126] Zhang Y, Fan Q, Dong L, et al. Are “Higher-Order” and “Layer-wise Zig-Zag” Plate & Shell Theories Necessary for Functionally Graded Materials and Structures? 2016; 32.